

Radiative Energy Loss in a Dynamically Evolving Quark-Gluon Plasma

Bithika Karmakar

*Incubator of Scientific Excellence—Centre for Simulations of Superdense Fluids,
University of Wrocław, Wrocław 50-204, Poland*

Magdalena Djordjevic*

*Institute of Physics Belgrade, University of Belgrade, 11080 Belgrade, Serbia and
Serbian Academy of Sciences and Arts, 11000 Belgrade, Serbia*

(Dated: December 24, 2024)

We present a theoretical formalism for calculating first-order in opacity radiative energy loss, incorporating the spatial and temporal temperature evolution of the Quark-Gluon Plasma (QGP) in a finite-size QCD medium with dynamical (i.e., moving) constituents. The derived expressions allow for the inclusion of arbitrary temperature profiles, enabling detailed calculations of radiative energy loss across various evolution scenarios. This advancement is crucial for utilizing high- p_{\perp} observables to constrain QGP properties through precision QGP tomography.

I. INTRODUCTION

The suppression of high transverse momentum (p_{\perp}) hadrons in heavy-ion collisions is a powerful probe for understanding the properties of the Quark-Gluon Plasma (QGP) [1–4], a state of matter believed to have existed shortly after the Big Bang [5]. Jet quenching [2], observed in high- p_{\perp} R_{AA} [6–9], v_2 , and higher harmonics [10–14], is directly linked to the energy loss of fast partons as they traverse the QGP and can be used to probe the QGP properties [15–31]. Theoretical predictions of jet quenching rely heavily on precise calculations of medium-induced energy loss, traditionally performed under one or more simplifying assumptions—such as a constant-temperature QCD medium, static scattering centers, or vacuum-like propagators (see [32–41], as well as various extensions of these methods, e.g., [42–49]). While these approaches have provided valuable insights, they inherently limit the applicability of such studies, particularly in QGP tomography, where spatial and temporal variations in the medium’s temperature and the dynamic nature of QGP constituents are critical factors.

Our previous work laid the groundwork for understanding radiative and collisional energy loss

*Electronic address: magda@ipb.ac.rs

in a finite-size, finite-temperature QCD medium composed of dynamical (i.e., moving) QGP constituents [38, 39]. We demonstrated [50] that including these effects is essential for accurately describing the interactions of high- p_{\perp} partons with the QGP formed in UltraRelativistic Heavy Ion Collisions (URHIC). While these findings are crucial for mapping out the dense QCD plasma created at the Large Hadron Collider (LHC) and the Relativistic Heavy Ion Collider (RHIC), they were developed under the assumption of a constant-temperature QGP and thus do not fully capture the complexity of a realistic, evolving QGP medium.

This manuscript extends our dynamical energy loss formalism [38, 39] to incorporate the effects of an evolving QGP on radiative energy loss, considering temperature variations under local equilibrium assumptions. This extension is essential for modeling energy loss in a medium where temperature varies with both position and time, aligning the formalism more closely with the conditions encountered in RHIC and LHC experiments, where the QGP undergoes spatial and temporal evolution.

Building on the dynamical energy loss formalism from our earlier works, we derive energy loss expressions by calculating all relevant Feynman diagrams in a finite-size QGP using finite temperature field theory and the Hard Thermal Loop (HTL) approach, and assuming local thermal equilibrium. This new formalism allows detailed calculations of radiative energy loss for arbitrary, spatially, and temporally varying temperature profiles, enabling high- p_{\perp} observables to be used as precision tools for constraining QGP properties through tomography, as outlined in the Conclusion.

The structure of this paper is as follows: In the Methods and Results section, we derive the first-order in opacity medium-induced radiative energy loss expression under the assumption of a temperature-evolving QCD medium. The assumptions behind our calculations are presented in Appendix A, with detailed calculations of contributing Feynman diagrams in Appendices B-M. To facilitate the derivation of results, we follow the procedure and notation from [38, 39], allowing for direct comparison and enabling readers to track the step-by-step inclusion of medium evolution into the dynamical energy loss formalism. While there are overlaps in methodology and figures, this approach ensures that the transition to a more complex, temperature-evolving medium is clear and accessible. In the Conclusion, we explore the implications of our results for QGP tomography, summarize our findings, and provide an outlook for further research.

II. METHODS AND RESULTS

A. Medium-Induced Radiation Spectrum

This section outlines the calculation of the medium-induced radiation spectrum for a high- p_\perp parton (jet). We consider a high- p_\perp parton produced at $\tau_0 = 0$ at an arbitrary position (x_0, y_0) , propagating in an arbitrary direction characterized by the angle ϕ . While the specific initial temperature $T(x_0, y_0)$ and jet direction are not the primary focus in this study, they serve as starting parameters for describing the temperature evolution along the jet's path. As the jet propagates through the medium, it encounters a temperature profile that evolves as $T(x_0 + \tau \cos \phi, y_0 + \tau \sin \phi)$, where τ represents the proper time [18].

When the temperature experienced by the high- p_\perp parton drops below the transition temperature $T_c = 155$ MeV [51], we assume that the jet has exited the QGP [18]. At this point, the calculation of the energy loss is terminated. The total path-length L of the high- p_\perp parton in this study corresponds to the distance traveled by the parton from its creation point (x_0, y_0) at $\tau_0 = 0$ until it leaves the medium, i.e., until the condition $T(x_0 + \tau \cos \phi, y_0 + \tau \sin \phi) < T_c$ is met.

This derivation focuses solely on the dependence of energy loss on the temperature profile along the jet's path, without delving into the specifics of initial conditions or jet orientation. Such a general treatment provides a robust analytical baseline, essential for developing frameworks like DREENA [17, 18] to calculate high- p_\perp observables. For the above expressions, the position along the trajectory is directly proportional to the proper time τ . Consequently, we introduce the integration variable $d\tau$, where τ represents the proper time along the path of the high- p_\perp parton.

Medium-induced radiative energy loss arises from gluon radiation caused by collisional interactions between a high- p_\perp parton and the medium. In this study, we derive the first-order opacity radiative energy loss, considering a single collisional interaction between the high- p_\perp parton and the medium, accompanied by the emission of one gluon [38, 39].

As in [38, 39, 52], we describe the medium as a quark-gluon plasma at temperature T and zero baryon density, consisting of n_f effective massless quark flavors in equilibrium with gluons. The key distinction between [38, 39] and this study lies in the treatment of the medium's thermal equilibrium. In [38, 39], a global thermal equilibrium was assumed, where the temperature T is constant throughout the QGP evolution. In contrast, this study accounts for local thermal equilibrium, incorporating temperature variations as the QGP evolves in space and time.

The formalism for energy loss in a finite-size dynamical QCD medium is detailed in Appendices B-L, where the diagrams are evaluated using finite-temperature field theory [53, 54] and HTL-resummed

propagators [54].

In Appendices B-L, we provide analytical derivations for 24 Feynman diagrams [38] that contribute to the first-order opacity energy loss. Each diagram represents a jet source J producing a high- p_\perp parton, which subsequently radiates a gluon with momentum $k = (\omega, k_z, \mathbf{k})$ while exchanging a virtual gluon of momentum $q = (q_0, q_z, \mathbf{q})$ with the medium. The jet emerges with momentum $p = (E, p_z, \mathbf{p})$. Following [35], we assume J varies slowly with momentum, so $J(p + k + q) \approx J(p + k) \approx J(p)$. Since the high- p_\perp parton is produced at $\tau = 0$, it can initially be either on-shell or off-shell, allowing more than one cut of the diagram to contribute to the energy loss, as detailed in the Appendices. These cuts interfere with each other, contributing to the Landau-Pomeranchuk-Migdal (LPM) effect [55] at high jet energies.

B. HTL Propagators

The HTL gluon propagator accounts for both transverse and longitudinal components [56–59] and is expressed as:

$$iD^{\mu\nu}(l) = \frac{P^{\mu\nu}(l)}{l^2 - \Pi_T(l)} + \frac{Q^{\mu\nu}(l)}{l^2 - \Pi_L(l)}, \quad (1)$$

where $l = (l_0, \vec{l})$ is the 4-momentum of the gluon. The transverse and longitudinal projection tensors, $P_{\mu\nu}(l)$ and $Q_{\mu\nu}(l)$, are associated with the transverse (Π_T) and longitudinal (Π_L) form factors of the HTL gluon self-energy, given by:

$$\Pi_T(l) = \mu^2 \left[\frac{y^2}{2} + \frac{y(1-y^2)}{4} \ln \left(\frac{y+1}{y-1} \right) \right], \quad \Pi_L(l) = \mu^2 \left[1 - y^2 - \frac{y(1-y^2)}{2} \ln \left(\frac{y+1}{y-1} \right) \right], \quad (2)$$

where $y \equiv l_0/|\vec{l}|$ and μ is the Debye screening mass.

To simplify the calculations, we work in the Coulomb gauge, where the non-zero components of the projection tensors reduce to:

$$P^{ij}(l) = -\delta^{ij} + \frac{l^i l^j}{\vec{l}^2}, \quad Q^{00}(l) = -\frac{l^2}{\vec{l}^2} = 1 - \frac{l_0^2}{\vec{l}^2} = 1 - y^2. \quad (3)$$

The exchanged gluon carries spacelike momentum [60–62], so only the Landau damping contribution ($q_0 \leq |\vec{q}|$) from the cut HTL effective propagator $D(q)$ [60, 61, 63] is relevant. Conversely, the radiated gluon has timelike momentum $k = (\omega, \vec{k})$, and its amplitude involves the quasi-particle contribution for $\omega > |\vec{k}|$ from the cut propagator $D(k)$ [53, 54, 64], which naturally separates these two contributions in momentum space.

C. Gluon Radiation Spectrum in a Locally Thermalized, Temperature-Evolving Medium

We use the same kinematic approximations as in [34–38], assuming the validity of the soft gluon ($\omega \ll E$) and soft rescattering ($\omega \gg |\vec{k}| \sim |\vec{q}| \sim q_0, q_z$) limits. After evaluating the diagrams detailed in Appendices B-L, the interaction rate is given as:

$$\Gamma(E) = \frac{1}{N_J} M_{tot} = \frac{1}{N_J} (M_{1,0} + M_{1,1} + M_{1,2}), \quad (4)$$

where $M_{1,0}$, $M_{1,1}$, and $M_{1,2}$ correspond to contributions with zero, one, or two ends of the exchanged gluon q connected to the radiated gluon k . The invariant distribution of jets N_J , determined by the effective jet source current [35], is:

$$N_J = D_R \int \frac{d^3p}{(2\pi)^3 2E} |J(p)|^2, \quad (5)$$

where $D_R = 3$ accounts for the jet colors.

The results for $M_{1,0}$, after combining Eqs. (B26)-(F3), are:

$$\begin{aligned} M_{1,0} &= \int_0^L d\tau \int \frac{d^3p}{(2\pi)^3 2E} |J(p)|^2 \int \frac{d^3k}{(2\pi)^3 2\omega} \int \frac{d^2q}{(2\pi)^2} 4g^4 [t_a, t_c] [t_c, t_a] T v(q, T) \\ &\times \frac{\mathbf{k}^2}{(\mathbf{k}^2 + \chi(T))^2} \left(1 - \cos(\xi(T)\tau) \right), \end{aligned} \quad (6)$$

or equivalently:

$$\begin{aligned} M_{1,0} &= D_R \int_0^L d\tau \int \frac{d^3p}{(2\pi)^3 2E} |J(p)|^2 \int \frac{dx}{x} \frac{d^2k}{\pi} \frac{d^2q}{\pi} \frac{C_R \alpha_s}{\pi} C_2(G) \alpha_s T v(q, T) \\ &\times \frac{\mathbf{k}^2}{(\mathbf{k}^2 + \chi(T))^2} \left(1 - \cos(\xi(T)\tau) \right), \end{aligned} \quad (7)$$

where $\chi(T) \equiv M^2 x^2 + m_g^2(T)$, $\xi(T) \equiv \frac{\vec{k}^2 + \chi(T)}{xE^+}$, and $v(q, T)$ is the effective potential. Here, we used $[t_a, t_c] [t_c, t_a] = C_2(G) C_R D_R$, with $C_2(G) = 3$, $C_R = 4/3$, and $D_R = 3$. In all expressions in this manuscript, we note that the temperature T is defined as in Subsection IIA, from which we see that it explicitly depends on the proper time τ .

Similarly, the results for $M_{1,1}$, obtained from Eqs. (G16)-(J9), are:

$$\begin{aligned} M_{1,1} &= 2D_R \int_0^L d\tau \int \frac{d^3p}{(2\pi)^3 2E} |J(p)|^2 \int \frac{dx}{x} \frac{d^2k}{\pi} \frac{d^2q}{\pi} \frac{C_R \alpha_s}{\pi} C_2(G) \alpha_s T v(q, T) \\ &\times \frac{-\mathbf{k} \cdot (\mathbf{k} + \mathbf{q})}{(\mathbf{k}^2 + \chi(T))((\mathbf{k} + \mathbf{q})^2 + \chi(T))} \left(1 - \cos(\zeta(T)\tau) \right), \end{aligned} \quad (8)$$

where $\zeta(T) \equiv \frac{(\mathbf{k} + \mathbf{q})^2 + \chi(T)}{xE^+}$.

Finally, combining Eqs. (K3) and (L4), $M_{1,2}$ becomes:

$$M_{1,2} = D_R \int_0^L d\tau \int \frac{d^3p}{(2\pi)^3 2E} |J(p)|^2 \int \frac{dx}{x} \frac{d^2k}{\pi} \frac{d^2q}{\pi} \frac{C_R \alpha_s}{\pi} C_2(G) \alpha_s T v(q, T) \\ \times \left[\frac{2(\mathbf{k} + \mathbf{q})^2}{((\mathbf{k} + \mathbf{q})^2 + \chi(T))^2} \left(1 - \cos(\zeta(T)\tau)\right) - \frac{\mathbf{k}^2}{(\mathbf{k}^2 + \chi(T))^2} \left(1 - \cos(\xi(T)\tau)\right) \right]. \quad (9)$$

Using Eqs. (5)-(9), the interaction rate reduces to:

$$\Gamma(E) = \int_0^L d\tau \int \frac{dx}{x} \frac{d^2k}{\pi} \frac{d^2q}{\pi} \frac{C_R \alpha_s}{\pi} C_2(G) \alpha_s T v(q, T) \\ \times \frac{2(\mathbf{k} + \mathbf{q})}{(\mathbf{k} + \mathbf{q})^2 + \chi(T)} \left(\frac{\mathbf{k} + \mathbf{q}}{(\mathbf{k} + \mathbf{q})^2 + \chi(T)} - \frac{\mathbf{k}}{\mathbf{k}^2 + \chi(T)} \right) \left(1 - \cos(\zeta(T)\tau)\right), \quad (10)$$

leading to the differential gluon radiation spectrum:

$$\frac{d^2 N_{\text{rad}}}{dx d\tau} = \int \frac{d^2k}{\pi} \frac{d^2q}{\pi} \frac{1}{x} \frac{C_R \alpha_s}{\pi} C_2(G) \alpha_s T v(q, T) \\ \times \frac{2(\mathbf{k} + \mathbf{q})}{(\mathbf{k} + \mathbf{q})^2 + \chi(T)} \left(\frac{\mathbf{k} + \mathbf{q}}{(\mathbf{k} + \mathbf{q})^2 + \chi(T)} - \frac{\mathbf{k}}{\mathbf{k}^2 + \chi(T)} \right) \left(1 - \cos(\zeta(T)\tau)\right). \quad (11)$$

By assuming a constant temperature and integrating over τ , this expression directly reproduces the gluon radiation spectrum from [38].

D. Generalization Towards Magnetic Screening and Running Coupling

As noted in [38], in the pure HTL approach, each diagram contributing to energy loss in a finite-size dynamical QCD medium is logarithmically divergent as the transverse momentum of the exchanged gluon approaches zero, *i.e.*, $\mathbf{q} \rightarrow 0$. This divergence arises from the contribution of transverse gluon exchange to radiative energy loss [65]. While Debye screening renders the longitudinal exchange infrared finite, the transverse exchange leads to a well-known logarithmic singularity due to the lack of magnetic screening [54] in the HTL approach. However, the infrared divergences are naturally regulated when all diagrams are accounted for, as shown in [38].

Different non-perturbative approaches [66–68] suggest a non-zero magnetic mass at RHIC and LHC. Non-perturbative effects are, therefore, important for a realistic description of energy loss interactions suitable for QGP tomography. In [69], we generalized the energy loss formalism to consistently include non-zero magnetic screening, modifying the HTL effective potential $v(q, T)$ from

$$\frac{\mu(T)^2}{\mathbf{q}^2 (\mathbf{q}^2 + \mu(T)^2)} \rightarrow \frac{\mu_E(T)^2}{(\mathbf{q}^2 + \mu_E(T)^2) (\mathbf{q}^2 + \mu_M(T)^2)}, \quad (12)$$

where $\mu_E(T)$ and $\mu_M(T)$ represent the electric and magnetic screening masses, respectively, with the magnetic-to-electric mass ratio approximately given by $\mu_M(T)/\mu_E(T) \approx 0.6$ [68].

The electric screening (Debye mass) $\mu_E(T)$ is self-consistently determined by solving the expression from [70]:

$$\frac{\mu_E(T)^2}{\Lambda_{QCD}^2} \ln \left(\frac{\mu_E(T)^2}{\Lambda_{QCD}^2} \right) = \frac{1 + N_f/6}{11 - 2/3 N_f} \left(\frac{4\pi T}{\Lambda_{QCD}} \right)^2, \quad (13)$$

leading to [29]

$$\mu_E = \sqrt{\Lambda^2 \frac{\psi(T)}{W(\psi(T))}}, \quad (14)$$

where

$$\psi(T) = \frac{1 + \frac{n_f}{6}}{11 - \frac{2}{3}n_f} \left(\frac{4\pi T}{\Lambda} \right)^2, \quad (15)$$

and W is Lambert's W function, while Λ_{QCD} is the perturbative QCD scale. This procedure ensures that $\mu_E(T)$ is consistent with lattice QCD [70].

Although the derivations in the appendices assume constant coupling, we include the running coupling $\alpha_S(Q^2)$, defined as [71]:

$$\alpha_S(Q^2) = \frac{4\pi}{(11 - 2/3 N_f) \ln(Q^2/\Lambda_{QCD}^2)}, \quad (16)$$

where the coupling enters the radiative energy loss expression as $\alpha_S(ET) \alpha_S(\frac{\mathbf{k}^2 + \chi(T)}{x})$ (see also [72]).

By incorporating these considerations into Eq. (11), the radiation spectrum becomes:

$$\begin{aligned} \frac{d^2 N_{\text{rad}}}{dx d\tau} &= \int \frac{d^2 k}{\pi} \frac{d^2 q}{\pi} \frac{2 C_R C_2(G) T}{x} \frac{\alpha_S(ET) \alpha_S(\frac{\mathbf{k}^2 + \chi(T)}{x})}{\pi} \frac{\mu_E(T)^2 - \mu_M(T)^2}{(\mathbf{q}^2 + \mu_M(T)^2)(\mathbf{q}^2 + \mu_E(T)^2)} \\ &\times \frac{(\mathbf{k} + \mathbf{q})}{(\mathbf{k} + \mathbf{q})^2 + \chi(T)} \left(\frac{(\mathbf{k} + \mathbf{q})}{(\mathbf{k} + \mathbf{q})^2 + \chi(T)} - \frac{\mathbf{k}}{\mathbf{k}^2 + \chi(T)} \right) \left(1 - \cos \left(\frac{(\mathbf{k} + \mathbf{q})^2 + \chi(T)}{xE^+} \tau \right) \right), \quad (17) \end{aligned}$$

which represents the evolution-dependent expression used to further develop the QGP tomography framework, DREENA [17, 18].

This study does not include numerical analyses of energy loss or the radiation spectrum, as these are inputs to the DREENA framework [17, 18], a tool for studying the properties of QGP [26–29]. Detailed numerical results can be found in the original references [17, 18]. Instead, this work focused on deriving the radiation spectrum expression in an evolving medium, which is a key component of the DREENA framework. The full derivation, presented in the Appendices for the first time, addresses an important methodological aspect and provides deeper insights into energy loss in an evolving QGP medium.

III. CONCLUSION

In this work, we have extended our previously developed dynamical energy loss formalism to include the space-time temperature evolution of QGP. This extension naturally incorporates temperature evolution within the dynamical energy loss framework, which is essential for accurate QGP tomography. By allowing for arbitrary spatial and temporal temperature profiles, the presented formalism offers a more realistic treatment of the QGP medium as encountered in heavy-ion collisions.

The derived energy loss expression has been successfully integrated into our DREENA framework, designed for precision QGP tomography. DREENA allowed us to constrain bulk QGP parameters by combining low- p_{\perp} and high- p_{\perp} theory with experimental data, providing new insights into the properties of this extreme state of matter. The ability of the framework to account for arbitrary temperature evolution significantly enhances its accuracy and applicability to experimental data from RHIC and LHC, marking a substantial advancement in our understanding of jet-medium interactions and the properties of the QGP.

Acknowledgments

We thank Igor Salom for valuable discussions. This work is supported by the European Research Council, grant ERC-2016-COG: 725741, and by the Ministry of Science and Technological Development of the Republic of Serbia. BK was also supported by the program Excellence Initiative—Research University of the University of Wrocław of the Ministry of Education and Science.

Appendix A: Notation, assumptions and the propagators

In the following appendices, we perform the calculations using light-cone coordinates [73]. The light-cone space-time coordinates $[x^+, x^-, \mathbf{x}]$ and momentum coordinates $[p^+, p^-, \mathbf{p}]$ are related to the laboratory frame coordinates (t, z, \mathbf{x}) and (E, p_z, \mathbf{p}) as follows:

$$x^+ = (t + z), \quad x^- = (t - z), \quad (\text{A1})$$

$$p^+ = (E + p_z), \quad p^- = (E - p_z), \quad (\text{A2})$$

where \mathbf{x} and \mathbf{p} are the transverse coordinates.

We consider a quark jet of finite mass M and large spatial momentum $p' \gg M$, produced inside the medium at the point x_0 . For simplicity, we choose the initial momentum of the quark jet to be aligned

along the z -axis:

$$p' = [E'^+, p'^-, \mathbf{0}]. \quad (\text{A3})$$

We consider the momentum of the virtual exchanged gluon and the radiated real gluon to be, respectively:

$$q = [q^+, q^-, \mathbf{q}] = (q_0, \vec{\mathbf{q}}) = (q_0, q_z, \mathbf{q}), \quad q_0 \leq |\vec{\mathbf{q}}|, \quad (\text{A4})$$

$$k = [k^+, k^-, \mathbf{k}] = (k_0, \vec{\mathbf{k}}) = (k_0, k_z, \mathbf{k}), \quad k_0 \geq |\vec{\mathbf{k}}|. \quad (\text{A5})$$

We assume the validity of the soft gluon ($\omega \ll E$) and soft rescattering ($|\mathbf{q}| \sim |\mathbf{k}| \ll k_z$) approximations [34–38]. Together with the conservation of energy and momentum ($p' = p + k + q$), one obtains:

$$p = \left[E^+, p^- = \frac{\mathbf{p}^2 + M^2}{E^+}, \mathbf{p} \right]. \quad (\text{A6})$$

For the calculation of the Feynman diagrams in Appendices B-L, we require the light-cone propagators $G_{++}^+(x)$, $G_{--}^-(x)$, and $G_{-+}(x)$ (the latter not being in light-cone coordinates) for the quark jet p , the radiated gluon k , and the exchanged gluon q . The relevant propagators are derived in Ref. [38]. The propagators for the exchanged gluon are given by:

$$D_{++}^{+\mu\nu}(x_i - x_j) = D_{--}^{-\mu\nu}(x_i - x_j) \approx D_{+-}^{\mu\nu}(x_i - x_j) \approx \int \frac{d^4 q}{(2\pi)^4} D_{\mu\nu}^> e^{-iq(x_i - x_j)}, \quad (\text{A7})$$

where $D^>(q, T)$ is the effective 1-HTL cut gluon propagator for the exchanged gluon [52]:

$$D_{\mu\nu}^>(q, T) = \theta \left(1 - \frac{q_0^2}{\vec{\mathbf{q}}^2} \right) (1 + f(q_0, T)) 2 \text{Im} \left(\frac{P_{\mu\nu}(q)}{q^2 - \Pi_T(q, T)} + \frac{Q_{\mu\nu}(q)}{q^2 - \Pi_L(q, T)} \right), \quad (\text{A8})$$

where $f(q_0, T) = (e^{q_0/T} - 1)^{-1}$. $\Pi_T(q, T)$ and $\Pi_L(q, T)$ (see Eq. (2)) are the transverse and longitudinal gluon self-energies, respectively. Additionally, $P_{\mu\nu}$ and $Q_{\mu\nu}$ represent the transverse and longitudinal projectors of the HTL gluon self-energy, respectively.

Since the exchanged gluons are virtual, with momentum given in Eq. (A4), only the Landau damping contribution from the gluon spectral function contributes to the above propagator.

In a finite-temperature QCD medium, the relevant radiative gluon propagator can be simplified as [64]:

$$D_{++}^{+\mu\nu}(x_i - x_j) = D_{--}^{-\mu\nu}(x_i - x_j) = \int \frac{dk^+ d^2 k}{(2\pi)^3 2k^+} \theta(k^+) P^{\mu\nu}(k) e^{-ik(x_i - x_j)} \quad (\text{A9})$$

$$D_{-+}^{\mu\nu}(x_i - x_j) = \int \frac{d^3 k}{(2\pi)^3 2\omega} P^{\mu\nu}(k) e^{-ik(x_i - x_j)}, \quad (\text{A10})$$

where $\omega(T) \approx \sqrt{\mathbf{k}^2 + m_g^2(T)}$ and $k^+ = \omega + k_z$. The gluon mass is given by $m_g(T) \approx \mu(T)/\sqrt{2}$ [64], with $\mu(T)$ being the Debye mass. The four-momentum k can then be expressed as:

$$k = \left[k^+, k^- = \frac{\mathbf{k}^2 + m_g^2(T)}{k^+}, \mathbf{k} \right]. \quad (\text{A11})$$

The relevant propagators for the quark jet are given by:

$$\Delta_{++}^+(x_i - x_j) = \Delta_{--}^-(x_i - x_j) = \int \frac{dp^+ d^2p}{(2\pi)^3 2p^+} \theta(p^+) e^{-ip(x_i - x_j)} \quad (\text{A12})$$

$$\Delta_{-+}(x_i - x_j) = \int \frac{d^3p}{(2\pi)^3 2E} e^{-ip(x_i - x_j)}. \quad (\text{A13})$$

Furthermore, in [52], it was shown that it is reasonable to assume $q_z \sim |\mathbf{q}|$. Since $|\mathbf{k}| \ll k_z$ and $q_z \sim |\mathbf{q}| \sim |\mathbf{k}|$, we then have $q_z \ll k_z$. Therefore, we get $k_z + q_z \approx k_z$ and $p_z + k_z + q_z \approx p_z + k_z \approx p_z + q_z \approx p_z$. Now, we define:

$$x \equiv \frac{k^+}{E^+} \approx \frac{(k+q)^+}{(E+q)^+}. \quad (\text{A14})$$

We further define $\chi(T)$, $\xi(T)$, and $\zeta(T)$ as:

$$\begin{aligned} \chi(T) &\equiv M^2 x^2 + m_g^2(T) \\ \xi(T) &\equiv \frac{\mathbf{k}^2 + \chi(T)}{xE^+} \\ \zeta(T) &\equiv \frac{(\mathbf{k}+\mathbf{q})^2 + \chi(T)}{xE^+} \\ \zeta(T) - \xi(T) &= \frac{(\mathbf{k}+\mathbf{q})^2 - \mathbf{k}^2}{xE^+}. \end{aligned} \quad (\text{A15})$$

Finally, since $\xi(T), \zeta(T) \ll |\mathbf{k}| \sim |\mathbf{q}|$, and $q_z \sim |\mathbf{q}| \sim |\mathbf{k}|$, we obtain $\xi(T), \zeta(T) \ll q_z$, which leads to the following relations:

$$\begin{aligned} q^- + \xi(T) &= q^0 - (q_z - \xi(T)) \approx q^0 - q_z \\ q^- + \zeta(T) &= q^0 - (q_z - \zeta(T)) \approx q^0 - q_z \\ q^- \pm (\zeta - \xi(T)) &= q^0 - (q_z \pm (\xi(T) - \zeta(T))) \approx q^0 - q_z. \end{aligned} \quad (\text{A16})$$

For clarity in presenting the cumbersome expressions in Appendices B-L, we will not always explicitly indicate the T dependence in ω , m_g , μ , χ , ξ , ζ , $D^>(q)$; however, it is understood that these variables depend on T . We assume that the QGP is in local equilibrium, meaning the temperature changes gradually with position and time. This study analytically derives the energy loss along the jet's path, focusing on the temperature profile's dependence on proper time τ . Since the position along the jet's trajectory is directly proportional to τ , the temperature T in this study depends only on τ , as described in Subsection IIA.

To simplify the comparison between constant T and evolving T medium, in the following appendices, we keep the same notation and structure of the Feynman diagrams as in [38]. In all Appendices, the diagrams are labeled as follows: In $M_{1,i,j,C}$, the number 1 indicates contributions to the energy loss at first order in opacity; i specifies how many ends of the virtual gluon q are connected to the radiated gluon k ; and j identifies the specific diagram within that class. The letter C indicates the central cut of the diagram, while in subsequent sections, the letters R and L will denote right and left cuts, respectively. Also, similar to Ref. [38], the calculations in Appendices B-L are performed under the assumption of a perturbative high-temperature QGP.

Appendix B: Calculation of Diagram $M_{1,0,1,C}$

In Appendices B-F, we compute the amplitudes of diagrams where both ends of the exchanged gluon q are attached to the jet, *i.e.*, neither end is connected to the radiated gluon k , and no three-gluon vertex is involved. This appendix presents the calculation of the diagram shown in Fig. 1.

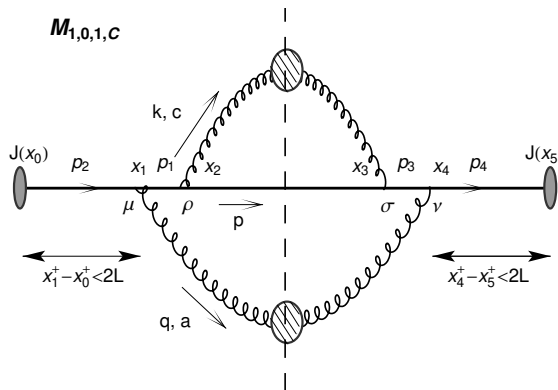


FIG. 1: Feynman diagram $M_{1,0,1,C}$, contributing to radiative energy loss at first order in opacity. The left (right) gray ellipse represents the source J , which produces a high- p_{\perp} parton with momentum p_2 (p_5) at time x_0 (x_5). Large dashed circles denote effective HTL gluon propagators [64]. The cut gluon propagators with momenta k and q correspond to the radiated gluon and a collisional interaction with a parton in the medium, respectively. Specific time points are denoted by x_i . Calculations are performed in the light cone coordinate system, with conditions $x_1^+ - x_0^+ < 2L$ and $x_5^+ - x_4^+ < 2L$, ensuring that the collisional interaction occurs before the high- p_{\perp} parton exits the QGP. The total path-length L traversed by the high- p_{\perp} parton represents the distance traveled from its creation point (x_0, y_0) at $\tau_0 = 0$ until the condition $T(x_0 + \tau \cos \phi, y_0 + \tau \sin \phi) < T_c$ is satisfied.

$$\begin{aligned}
M_{1,0,1,C} &= \int \prod_{i=0}^5 d^4 x_i J(x_0) \Delta_{++}^+(x_1 - x_0) v_{\mu}^+(x_1) D_{-+}^{\mu\nu}(x_4 - x_1) \Delta_{++}^+(x_2 - x_1) v_{\rho}^+(x_2) \\
&\quad \times D_{-+}^{\rho\sigma}(x_3 - x_2) \Delta_{-+}(x_3 - x_2) v_{\sigma}^-(x_3) \Delta_{--}^-(x_4 - x_3) v_{\nu}^-(x_4) \Delta_{--}^-(x_5 - x_4) J(x_5) \\
&\quad \times \theta(x_1^+ - x_0^+) \theta(x_2^+ - x_1^+) \theta(2L - (x_1^+ - x_0^+)) \theta(x_4^+ - x_5^+) \theta(x_3^+ - x_4^+) \\
&\quad \times \theta(2L - (x_4^+ - x_5^+)). \tag{B1}
\end{aligned}$$

Here J represents the source of the jet, Δ corresponds to the jet propagator, D denotes the gluon propagators, and v represents the vertices. Using the expressions for the propagators provided in the previous section, we obtain:

$$\begin{aligned}
M_{1,0,1,C} &= \int \prod_{i=0}^5 d^4 x_i J(x_0) \int_{-\infty}^{\infty} \int_0^{\infty} \frac{dp_2^+ d^2 p_2}{(2\pi)^3 2p_2^+} e^{-ip_2 \cdot (x_1 - x_0)} \int \frac{d^4 q}{(2\pi)^4} D_{\mu\nu}^>(q, T) e^{-iq(x_4 - x_1)} \\
&\quad \times \int_{-\infty}^{\infty} \int_0^{\infty} \frac{dp_1^+ d^2 p_1}{(2\pi)^3 2p_1^+} e^{-ip_1 \cdot (x_2 - x_1)} (-ig(p_2 + p_1)^{\mu} t_a) \\
&\quad \times (-1) \int \frac{d^3 k}{(2\pi)^3 2\omega} P_{\rho\sigma}(k) e^{-ik \cdot (x_3 - x_2)} \int \frac{d^3 p}{(2\pi)^3 2E} e^{-ip \cdot (x_3 - x_2)} (-ig(p_1 + p)^{\rho} t_c) \\
&\quad \times \int_{-\infty}^{\infty} \int_0^{\infty} \frac{dp_3^+ d^2 p_3}{(2\pi)^3 2p_3^+} e^{-ip_3 \cdot (x_4 - x_3)} (ig(p + p_3)^{\sigma} t_c) \int_{-\infty}^{\infty} \int_0^{\infty} \frac{dp_4^+ d^2 p_4}{(2\pi)^3 2p_4^+} e^{-ip_4 \cdot (x_5 - x_4)} \\
&\quad \times (ig(p_3 + p_4)^{\nu} t_a) J(x_5) \theta(x_1^+ - x_0^+) \theta(x_2^+ - x_1^+) \theta(2L - (x_1^+ - x_0^+)) \theta(x_4^+ - x_5^+) \\
&\quad \times \theta(x_3^+ - x_4^+) \theta(2L - (x_4^+ - x_5^+)) \\
&= \int_{-\infty}^{\infty} \int_0^{\infty} \prod_{i=1}^4 \frac{dp_i^+ d^2 p_i}{(2\pi)^3 2p_i^+} \int \frac{d^3 k}{(2\pi)^3 2\omega} \int \frac{d^3 p}{(2\pi)^3 2E} \int \frac{d^4 q}{(2\pi)^4} g^4 t_a t_c t_c t_a I \tag{B2}
\end{aligned}$$

where

$$\begin{aligned}
I &= \int \prod_{i=0}^5 d^4 x_i \theta(x_1^+ - x_0^+) \theta(x_2^+ - x_1^+) \theta(2L - (x_1^+ - x_0^+)) \theta(x_4^+ - x_5^+) \theta(x_3^+ - x_4^+) \\
&\quad \times \theta(2L - (x_4^+ - x_5^+)) e^{-ip_2 \cdot (x_1 - x_0)} e^{-iq \cdot (x_4 - x_1)} e^{-ip_1 \cdot (x_2 - x_1)} e^{-i(p+k) \cdot (x_3 - x_2)} e^{-ip_3 \cdot (x_4 - x_3)} \\
&\quad \times e^{-ip_4 \cdot (x_5 - x_4)} J(x_0) J(x_5) (p_1 + p_2)^{\mu} D_{\mu\nu}^>(q, T) (p_3 + p_4)^{\nu} (p + p_1)^{\rho} P_{\rho\sigma}(k) (p + p_3)^{\sigma} \\
&= |J(p)|^2 (2\pi)^3 \delta((p_2 - p - k - q)^+) \delta^2(\mathbf{p}_2 - \mathbf{p} - \mathbf{k} - \mathbf{q}) (2\pi)^3 \delta((p_1 - p - k)^+) \delta^2(\mathbf{p}_1 - \mathbf{p} - \mathbf{k}) \\
&\quad \times (2\pi)^3 \delta((p_3 - p - k)^+) \delta^2(\mathbf{p}_3 - \mathbf{p} - \mathbf{k}) (2\pi)^3 \delta((p_4 - p - k - q)^+) \delta^2(\mathbf{p}_4 - \mathbf{p} - \mathbf{k} - \mathbf{q}) I_1, \tag{B3}
\end{aligned}$$

where

$$\begin{aligned}
I_1 &= \int_0^{\infty} dx_2'^+ e^{-\frac{i}{2}(p_1 - p - k)^- x_2'^+} \int_0^{2L} dx_1'^+ e^{-\frac{i}{2}(p_2 - p - k - q)^- x_1'^+} \int_0^{\infty} dx_3'^+ e^{\frac{i}{2}(p_3 - p - k)^- x_3'^+} \\
&\quad \times \int_0^{2L} dx_4'^+ e^{\frac{i}{2}(p_4 - p - k - q)^- x_4'^+} (p_1 + p_2)^{\mu} D_{\mu\nu}^>(q, T) (p_3 + p_4)^{\nu} (p + p_1)^{\rho} P_{\rho\sigma}(k) (p + p_3)^{\sigma}. \tag{B4}
\end{aligned}$$

Here $x'_1 = x_1 - x_0$, $x'_2 = x_2 - x_1$, $x'_3 = x_3 - x_4$, $x'_4 = x_4 - x_5$.

By applying the δ functions from Eq. (B3) and using

$$p_i^- = \frac{\mathbf{p}_i^2 + M^2}{p_i^+}, \quad (\text{B5})$$

$$k^- = \frac{\mathbf{k}^2 + m_g(T)^2}{k^+}, \quad (\text{B6})$$

we obtain (noting that $\mathbf{p} + \mathbf{k} + \mathbf{q} = 0 \rightarrow \mathbf{p} + \mathbf{k} = -\mathbf{q}$):

$$p_1^- = p_3^- = \frac{\mathbf{q}^2 + M^2}{(p+k)^+}. \quad (\text{B7})$$

In the soft gluon and soft rescattering approximation, we find (where $x \equiv \frac{k^+}{E^+}$, and $\xi(T)$ and $\zeta(T)$ are defined in Eq. (A15)):

$$\begin{aligned} (p_1 - p - k)^- &= (p_3 - p - k)^- = \frac{\mathbf{k}^2 + \chi(T)}{xE^+} = -\xi(T), \\ (p_2 - p - k)^- &= \frac{(\mathbf{k} + \mathbf{q})^2 + \chi(T)}{xE^+} = -\zeta(T). \end{aligned} \quad (\text{B8})$$

Similarly, for highly energetic partons [38],

$$\begin{aligned} (p + p_1)^\rho P_{\rho\sigma}(k) (p + p_3)^\sigma &\approx -\frac{4\mathbf{k}^2}{x^2} \\ (p_1 + p_2)^\mu P_{\mu\nu}(q) (p_3 + p_4)^\nu &\approx -(p_1 + p_2)^\mu Q_{\mu\nu}(q) (p_3 + p_4)^\nu \approx -E^{+2} \frac{\mathbf{q}^2}{\mathbf{q}^2}, \end{aligned} \quad (\text{B9})$$

By using Eq. (B9) and Eq. (A8), $(p_1 + p_2)^\mu D_{\mu\nu}^>(q, T) (p_3 + p_4)^\nu$ becomes

$$\begin{aligned} (p_1 + p_2)^\mu D_{\mu\nu}^>(q, T) (p_3 + p_4)^\nu &\approx (p_1 + p_2)^\mu 2 \text{Im} \left(\frac{P_{\mu\nu}(q)}{q^2 - \Pi_T(q, T)} + \frac{Q_{\mu\nu}(q)}{q^2 - \Pi_L(q, T)} \right) (p_3 + p_4)^\nu \\ &\approx \theta \left(1 - \frac{q_0^2}{\mathbf{q}^2} \right) f(q_0, T) E^{+2} \frac{\mathbf{q}^2}{\mathbf{q}^2} 2 \text{Im} \left(\frac{1}{q^2 - \Pi_L(q, T)} - \frac{1}{q^2 - \Pi_T(q, T)} \right) \\ &\equiv F(q_0, q_z, \mathbf{q}, T), \end{aligned} \quad (\text{B10})$$

where $f(q_0, T) = (e^{q_0/T} - 1)^{-1}$. For small q_0 , $f(q_0, T)$ can be expanded to [52]

$$f(q_0, T) \sim T/q_0. \quad (\text{B11})$$

By using Eqs. (B5)-(B11), Eq. (B4) reduces to

$$\begin{aligned} I_1 &= 4 \int_0^\infty dx_2'^+ e^{-\frac{i}{2}\xi(T)x_2'^+} \int_0^\infty dx_3'^+ e^{\frac{i}{2}\xi(T)x_3'^+} \frac{-4\mathbf{k}^2}{x^2} \int_0^L dl_1 e^{i(\zeta(T)+q)l_1} \int_0^L dl_4 e^{-i(\zeta(T)+q^-)l_4} \\ &\quad \times \theta \left(1 - \frac{q_0^2}{\mathbf{q}^2} \right) \frac{T}{q_0} E^{+2} \frac{\mathbf{q}^2}{\mathbf{q}^2} 2 \text{Im} \left(\frac{1}{q^2 - \Pi_L(q, T)} - \frac{1}{q^2 - \Pi_T(q, T)} \right), \end{aligned} \quad (\text{B12})$$

where $l_1 = x_1'^+/2$ and $l_4 = x_4'^+/2$.

Further, by using soft gluon, soft rescattering approximation, we have $\zeta(T)+q^- \approx q^-$ [52]. Therefore,

$$I_1 = \frac{-16}{\xi(T)^2} \frac{4\mathbf{k}^2}{x^2} \int_0^L dl_1 e^{iq^-l_1} \int_0^L dl_4 e^{-iq^-l_4} \theta\left(1 - \frac{q_0^2}{\mathbf{q}^2}\right) E^{+2} \frac{\mathbf{q}^2}{\mathbf{q}^2} \times \frac{T}{q_0} 2 \operatorname{Im} \left(\frac{1}{q^2 - \Pi_L(q, T)} - \frac{1}{q^2 - \Pi_T(q, T)} \right), \quad (\text{B13})$$

where the second line of Eq. (B13) depends on the temperature T , which also affects $\xi(T)$, $\Pi_L(q, T)$, and $\Pi_T(q, T)$. Furthermore, the temperature dependence is associated with both l_1 and l_4 . However, since this is a cutoff diagram, l_1 and l_4 correspond to mirror images of the same position in space and time. Thus, we associate the temperature dependence with l_1 . Consequently, Eq. (B13) simplifies to

$$I_1 = \int_0^L dl_1 e^{iq^-l_1} \int_0^L dl_4 e^{-iq^-l_4} G(q, T(l_1)), \quad (\text{B14})$$

where

$$G(q, T(l_1)) = -\frac{16}{\xi(T)^2} \left(\frac{4\mathbf{k}^2}{x^2} \right) \theta\left(1 - \frac{q_0^2}{\mathbf{q}^2}\right) \frac{T}{q_0} E^{+2} \frac{\mathbf{q}^2}{\mathbf{q}^2} 2 \operatorname{Im} \left(\frac{1}{q^2 - \Pi_L(q, T)} - \frac{1}{q^2 - \Pi_T(q, T)} \right), \quad (\text{B15})$$

and, as noted above, T explicitly depends on l_1 .

To calculate the integrals in Eq. (B14), we note that this part corresponds to the collisional interaction between the jet and a medium parton [60]. For a constant temperature ($T = \text{const}$), $G(q, T)$ can be extracted from the integrals over l_1 and l_4 , simplifying Eq. (B14) to:

$$\begin{aligned} I_1^{\text{const}} &= G(q, T) \int_0^L dl_1 e^{iq^-l_1} \int_0^L dl_4 e^{iq^-l_4} \\ &= G(q, T) \frac{e^{iq^-L} - 1}{iq^-} \frac{e^{-iq^-L} - 1}{-iq^-} \\ &= G(q, T) \frac{2(1 - \cos(q^-L))}{(q^-)^2} \\ &= G(q, T) \frac{4 \sin^2\left(\frac{q^-L}{2}\right)}{(q^-)^2}. \end{aligned} \quad (\text{B16})$$

In Ref. [60], we showed that the finite size effects for collisional interactions are negligible, further reducing this expression to:

$$\lim_{L \rightarrow \infty} \frac{4 \sin^2\left(\frac{q^-L}{2}\right)}{(q^-)^2} = 2\pi L \delta(q^-). \quad (\text{B17})$$

To generalize our calculations from $T = \text{const}$ to the local equilibrium case, we still expect that finite

size effects for collisional interactions remain negligible. Therefore, I_1 becomes:

$$\begin{aligned}
I_1 &= \int_0^L \int_0^L dl_1 dl_4 G(q, T(l_1)) \left(\cos(q^- l_1) \cos(q^- l_4) + \sin(q^- l_1) \sin(q^- l_4) \right) \\
&= \int_0^L dl_1 G(q, T(l_1)) \cos(q^- l_1) \int_0^L dl_4 \cos(q^- l_4) \\
&\quad + \int_0^L dl_1 G(q, T(l_1)) \sin(q^- l_1) \int_0^L dl_4 \sin(q^- l_4) \\
&= \int_0^L dl_1 G(q, T(l_1)) \cos(q^- l_1) \frac{\sin(q^- L)}{q^-} - \int_0^L dl_1 G(q, T(l_1)) \sin(q^- l_1) \frac{1 - \cos(q^- L)}{q^-}.
\end{aligned} \tag{B18}$$

In the limit $L \rightarrow \infty$, $\frac{\sin(q^- L)}{q^-} = \pi \delta(q^-)$, leading to

$$\begin{aligned}
I_1 &= \pi \delta(q^-) \int_0^L dl_1 G(q, T(l_1)) \\
&\quad - \int_0^L dl_1 G(q, T(l_1)) \sin(q^- l_1) \frac{1 - \cos(q^- L)}{q^-}.
\end{aligned} \tag{B19}$$

Since we assume local equilibrium, for the second integral in Eq. (B19), we assume that $G(q, T(l_1))$ is a slowly changing function in position and time and can be replaced by $\langle G(q) \rangle = \frac{1}{L} \int_0^L dl_1 G(q, T(l_1))$.

Then the second integral in Eq. (B19) becomes:

$$\begin{aligned}
&- \int_0^L dl_1 G(q, T(l_1)) \sin(q^- l_1) \frac{1 - \cos(q^- L)}{q^-} \\
&\approx \int \frac{d^4 q}{(2\pi)^4} \langle G(q) \rangle \left(\frac{1 - \cos(q^- L)}{q^-} \right)^2 \\
&= \langle G(q) \rangle \left(\frac{\sin^2 \frac{q^- L}{2}}{(q^-)^2} - \frac{\sin^2(q^- L)}{(q^-)^2} \right) \\
&=_{L \rightarrow \infty} \langle G(q) \rangle (2\pi L \delta(q^-) - \pi L \delta(q^-)) \\
&= \langle G(q) \rangle \pi L \delta(q^-) \\
&\approx \int_0^L dl_1 G(q, T(l_1)) \pi \delta(q^-).
\end{aligned} \tag{B20}$$

This finally leads to:

$$I_1 = 2\pi \delta(q^-) \int_0^L dl_1 G(q, T(l_1)). \tag{B21}$$

This leads to the assumption for the collisional integral in Eq. (B14) as:

$$\int_0^L dl e^{iq^- l} \approx 2\pi \delta(q^-), \tag{B22}$$

which accounts for an additional factor of 2 in Eq. (B22) due to integration limits and symmetry considerations, as shown in Eqs. (B14)-(B22). This result will be used in subsequent diagram computations to avoid redundancy.

Therefore, $M_{1,0,1,C}$ reduces to:

$$M_{1,0,1,C} = \int_0^L d\tau \int \frac{d^3p}{(2\pi)^3 2E} |J(p)|^2 \int \frac{d^3k}{(2\pi)^3 2\omega} 4g^4 t_a t_c t_c t_a \frac{\mathbf{k}^2}{(\mathbf{k}^2 + \chi(T))^2} I_q(T), \quad (\text{B23})$$

where

$$I_q(T) = T \int \frac{d^4q}{(2\pi)^4} 2\pi \delta(q_0 - q_z) \frac{1}{q_0} \frac{\mathbf{q}^2}{\mathbf{q}^2} 2 \text{Im} \left(\frac{1}{q^2 - \Pi_L(q, T)} - \frac{1}{q^2 - \Pi_T(q, T)} \right). \quad (\text{B24})$$

Here, the variable l_1 is replaced with the directly proportional proper time τ , explicitly assuming that the temperature T depends on τ .

In the high-temperature limit, $I_q(T)$ reduces to (see Appendix C in Ref. [52] for more details):

$$I_q(T) = T \int \frac{d^2q}{(2\pi)^2} v(q, T), \quad (\text{B25})$$

where $v(q, T) = \frac{\mu^2(T)}{q^2(q^2 + \mu^2(T))}$ is the effective potential. Finally, Eq. (B23) becomes:

$$M_{1,0,1,C} = 4t_a t_c t_c t_a \int_0^L d\tau \int \frac{d^3p}{(2\pi)^3 2E} |J(p)|^2 \int \frac{d^3k}{(2\pi)^3 2\omega} \int \frac{d^2q}{(2\pi)^2} g^4 T v(q, T) \frac{\mathbf{k}^2}{(\mathbf{k}^2 + \chi(T))^2}. \quad (\text{B26})$$

Appendix C: Calculation of Diagrams $M_{1,0,2,C}$, $M_{1,0,2,R}$, and $M_{1,0,2,L}$

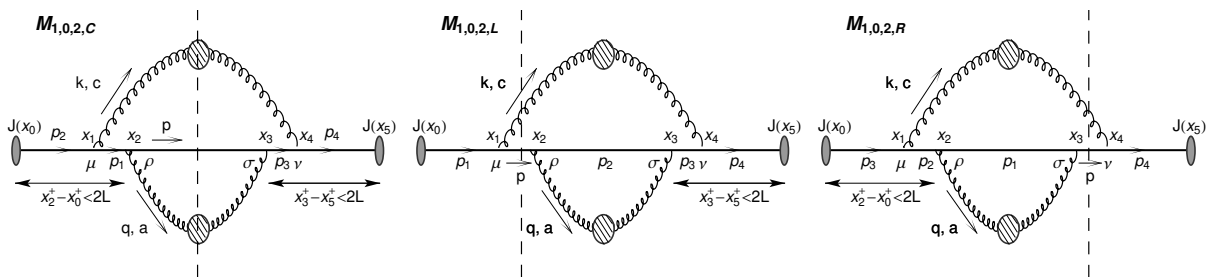


FIG. 2: Feynman diagrams $M_{1,0,2,C}$, $M_{1,0,2,L}$, and $M_{1,0,2,R}$, labeled equivalently to Fig. 1. The left, middle, and right panels depict three possible cuts (central, left, and right, respectively) of the same 2-HTL Feynman diagram, all contributing to the first-order in opacity radiative energy loss.

We will first calculate the cut diagram $M_{1,0,2,C}$, shown in the left panel of Fig. 2.

$$\begin{aligned}
M_{1,0,2,C} &= \int \prod_{i=0}^5 d^4 x_i J(x_0) \Delta_{++}^+(x_1 - x_0) v_\mu^+(x_1) D_{-+}^{\mu\nu}(x_4 - x_1) \Delta_{++}^+(x_2 - x_1) v_\rho^+(x_2) D_{-+}^{\rho\sigma}(x_3 - x_2) \\
&\quad \times \Delta_{-+}(x_3 - x_2) v_\sigma^-(x_3) \Delta_{--}^-(x_4 - x_3) v_\nu^-(x_4) \Delta_{--}^-(x_5 - x_4) J(x_5) \\
&\quad \times \theta(x_1^+ - x_0^+) \theta(x_2^+ - x_1^+) \theta(2L - (x_2^+ - x_0^+)) \theta(x_4^+ - x_5^+) \theta(x_3^+ - x_4^+) \theta(2L - (x_3^+ - x_5^+)) \\
&= - \int_{-\infty}^{\infty} \int_0^{\infty} \prod_{i=1}^4 \frac{dp_i^+ d^2 p_i}{(2\pi)^3 2p_i^+} \int \frac{d^3 k}{(2\pi)^3 2\omega} \int \frac{d^3 p}{(2\pi)^3 2E} \int \frac{d^4 q}{(2\pi)^4} g^4 t_c t_a t_a t_c I
\end{aligned} \tag{C1}$$

where

$$\begin{aligned}
I &= \int \prod_{i=0}^5 d^4 x_i \theta(x_1^+ - x_0^+) \theta(x_2^+ - x_1^+) \theta(2L - (x_2^+ - x_0^+)) \theta(x_4^+ - x_5^+) \theta(x_3^+ - x_4^+) \\
&\quad \times \theta(2L - (x_3^+ - x_5^+)) e^{-ip_2 \cdot (x_1 - x_0)} e^{-ik \cdot (x_4 - x_1)} e^{-ip_1 \cdot (x_2 - x_1)} e^{-i(p+q) \cdot (x_3 - x_2)} e^{-ip_3 \cdot (x_4 - x_3)} \\
&\quad \times e^{-ip_4 \cdot (x_5 - x_4)} J(x_0) J(x_5) (p_1 + p_2)^\mu P_{\mu\nu}(k) (p_3 + p_4)^\nu (p + p_1)^\rho D_{\rho\sigma}^>(q) (p + p_3)^\sigma \\
&= |J(p)|^2 (2\pi)^3 \delta((p_2 - p_1 - k)^+) \delta^2(\mathbf{p}_2 - \mathbf{p}_1 - \mathbf{k}) (2\pi)^3 \delta((p_1 - p - q)^+) \delta^2(\mathbf{p}_1 - \mathbf{p} - \mathbf{q}) \\
&\quad \times (2\pi)^3 \delta((p_3 - p - q)^+) \delta^2(\mathbf{p}_3 - \mathbf{p} - \mathbf{q}) (2\pi)^3 \delta((p_4 - p_3 - k)^+) \delta^2(\mathbf{p}_4 - \mathbf{p}_3 - \mathbf{k}) I_1,
\end{aligned} \tag{C2}$$

and where

$$\begin{aligned}
I_1 &= \int_0^{2L} dx_2'^+ e^{-\frac{i}{2}(p_1 - p - q)^- x_2'^+} \int_0^{x_2'^+} dx_1'^+ e^{-\frac{i}{2}(p_2 - p_1 - k)^- x_1'^+} \int_0^{2L} dx_3'^+ e^{\frac{i}{2}(p_3 - p - q)^- x_3'^+} \\
&\quad \times \int_0^{x_3'^+} dx_4'^+ e^{\frac{i}{2}(p_4 - p_3 - k)^- x_4'^+} (p_1 + p_2)^\mu P_{\mu\nu}(k) (p_3 + p_4)^\nu (p + p_1)^\rho D_{\rho\sigma}^>(q) (p + p_3)^\sigma.
\end{aligned} \tag{C3}$$

Here, we defined $x_1' = x_1 - x_0$, $x_2' = x_2 - x_0$, $x_3' = x_3 - x_5$, and $x_4' = x_4 - x_5$.

Now, by applying the δ functions from Eq. (C2), and using Eqs. (B5), (B6), we obtain $p_1^- = p_3^-$ and $p_2^- = p_4^-$.

Using Eqs. (B9) and (B10), I_1 becomes:

$$\begin{aligned}
I_1 &= 4 \int_0^L dl_2 e^{-i(p_1 - p - q)^- l_2} \int_0^{2l_2} dx_1'^+ e^{-\frac{i}{2}(p_2 - p_1 - k)^- x_1'^+} \int_0^L dl_3 e^{i(p_3 - p - q)^- l_3} \\
&\quad \times \int_0^{2l_3} dx_4'^+ e^{\frac{i}{2}(p_4 - p_3 - k)^- x_4'^+} \frac{-4\mathbf{k}^2}{x^2} \theta\left(1 - \frac{q_0^2}{\mathbf{q}^2}\right) \frac{T}{q_0} E^{+2} \frac{\mathbf{q}^2}{\mathbf{q}^2} \\
&\quad \times 2 \operatorname{Im} \left(\frac{1}{q^2 - \Pi_L(q, T)} - \frac{1}{q^2 - \Pi_T(q, T)} \right),
\end{aligned} \tag{C4}$$

where $l_2 = x_2'^+/2$ and $l_3 = x_3'^+/2$. Similar to Appendix B, the second line of Eq. (C4) depends on the temperature T through $\xi(T)$, $\Pi_L(q, T)$, and $\Pi_T(q, T)$. Furthermore, the temperature dependence is associated with both l_2 and l_3 . However, since this is a cutoff diagram, these two correspond to the mirror image of the same position in space and time, and we associate it with l_2 . Similar considerations are applied in further appendices as well.

In soft gluon, soft rescattering approximation

$$\begin{aligned} (p_1 - p)^- &\approx \frac{\mathbf{k}^2 - (\mathbf{k} + \mathbf{q})^2}{E^+} \\ (p_1 + k - p_2)^- &\approx \xi(T). \end{aligned} \quad (\text{C5})$$

Now, we perform the x_1^+ and x_4^+ integrations in Eq. (C4):

$$I_1 = \int_0^L dl_3 e^{-i(p_1-p-q)^-l_3} \left(1 - e^{i(p_1+k-p_2)^-l_3}\right) \int_0^L dl_2 e^{i(p_3-p-q)^-l_2} \left(1 - e^{-i(p_1+k-p_2)^-l_2}\right) G(q, T), \quad (\text{C6})$$

where $G(q, T)$ is defined in Eq. (B15).

Here, we note that the spacetime integrations over l_2 and l_3 correspond to the collisional interaction. We perform the l_3 integration using Eq. (B22), leading to:

$$\begin{aligned} I_1 &= 2\pi \int_0^L dl_2 \left[\delta((p_2 - p - k - q)^-) \left(1 - e^{i(p_1+k-p_2)^-l_2}\right) + \delta((p_1 - p - q)^-) \right. \\ &\quad \left. \times \left(1 - e^{-i(p_1+k-p_2)^-l_2}\right) \right] G(q, T(l_2)). \end{aligned} \quad (\text{C7})$$

Note that $(p_1 - p)^- \ll \xi(T) \ll |\mathbf{k}|, |\mathbf{q}|, q_z$, leading to:

$$\begin{aligned} (\delta((p_2 - p - k - q)^-) + \delta((p_1 - p - q)^-)) &\approx 2\delta((p_2 - p - k - q)^-) \approx 2\delta(q_0 - q_z), \\ (\delta((p_2 - p - k - q)^-) - \delta((p_1 - p - q)^-)) &\approx \delta(q_0 - q_z + \xi(T)) - \delta(q_0 - q_z). \end{aligned} \quad (\text{C8})$$

By using Eq. (C8), Eq. (C7) finally reduces to:

$$\begin{aligned} I_1 &= \frac{\pi}{2} \int_0^L d\tau \left[2\delta(q_0 - q_z) \left(1 - \frac{e^{-i\xi(T)\tau}}{2} - \frac{e^{i\xi(T)\tau}}{2}\right) + (\delta(q_0 - q_z + \xi(T)) - \delta(q_0 - q_z)) \right. \\ &\quad \left. \times \left(\frac{e^{-i\xi(T)\tau}}{2} - \frac{e^{i\xi(T)\tau}}{2}\right) \right] G(q, T), \end{aligned} \quad (\text{C9})$$

where, as in the previous section, the variable l_2 is here replaced with the directly proportional proper time τ , and we explicitly assume that the temperature T depends on τ .

By using Eqs. (C2) and (C9), and after performing integrations over p_1, p_2, p_3 , and p_4 , Eq. (C1) becomes:

$$\begin{aligned} M_{1,0,2,C} &= \int_0^L d\tau \int \frac{d^3p}{(2\pi)^3 2E} |J(p)|^2 \int \frac{d^3k}{(2\pi)^3 2\omega} 4g^4 t_c t_a t_a t_c \frac{\mathbf{k}^2}{(\mathbf{k}^2 + \chi(T))^2} \\ &\quad \times \left[2I_q(T) \left(1 - \frac{e^{-i\xi(T)\tau}}{2} - \frac{e^{i\xi(T)\tau}}{2}\right) + J_q(T) \left(\frac{e^{-i\xi(T)\tau}}{2} - \frac{e^{i\xi(T)\tau}}{2}\right) \right], \end{aligned} \quad (\text{C10})$$

where $I_q(T)$ is given by Eq. (B25), and

$$\begin{aligned} J_q(T) &= \int \frac{d^4q}{(2\pi)^4} 2\pi (\delta(q_0 - q_z + \xi(T)) - \delta(q_0 - q_z)) \frac{T}{q_0} \frac{\mathbf{q}^2}{\mathbf{q}^2} 2 \text{Im} \left(\frac{1}{q^2 - \Pi_L(q, T)} - \frac{1}{q^2 - \Pi_T(q, T)} \right) \\ &= \xi(T) \int \frac{d^3q}{(2\pi)^3} \frac{2\pi}{E^{+2}} \frac{dF(q_0, q_z, \mathbf{q}, T)}{dq_0} \Big|_{q_0=q_z} = 0, \end{aligned} \quad (\text{C11})$$

as $\left. \frac{dF(q_0, q_z, \mathbf{q}, T)}{dq_0} \right|_{q_0=q_z}$ is an odd function of q_z .

Finally, by using Eqs. (B25) and (C11), Eq. (C10) reduces to:

$$M_{1,0,2,C} = 8t_c t_a t_c \int_0^L d\tau \int \frac{d^3 p}{(2\pi)^3 2E} |J(p)|^2 \int \frac{d^3 k}{(2\pi)^3 2\omega} \int \frac{d^2 q}{(2\pi)^2} g^4 T v(q, T) \times \frac{\mathbf{k}^2}{(\mathbf{k}^2 + \chi(T))^2} \left(1 - \cos(\xi(T)\tau)\right). \quad (\text{C12})$$

Now we proceed with the cut diagrams $M_{1,0,2,L}$ and $M_{1,0,2,R}$, shown in the central and right panels of Fig. 2, respectively. We begin with $M_{1,0,2,R}$:

$$\begin{aligned} M_{1,0,2,R} &= \int \prod_{i=0}^5 d^4 x_i J(x_0) \Delta_{++}^+(x_1 - x_0) v_\mu^+(x_1) D_{-+}^{\mu\nu}(x_4 - x_1) \Delta_{++}^+(x_2 - x_1) v_\rho^+(x_2) \\ &\quad \times D_{++}^{+\rho\sigma}(x_3 - x_2) \Delta_{++}^+(x_3 - x_2) v_\sigma^+(x_3) \Delta_{-+}(x_4 - x_3) v_\nu^-(x_4) \Delta_{--}^-(x_5 - x_4) J(x_5) \\ &\quad \times \theta(x_1^+ - x_0^+) \theta(x_2^+ - x_1^+) \theta(x_3^+ - x_2^+) \theta(2L - (x_2^+ - x_0^+)) \theta(x_4^+ - x_5^+) \\ &= \int_{-\infty}^{\infty} \int_0^{\infty} \prod_{i=1}^4 \frac{dp_i^+ d^2 p_i}{(2\pi)^3 2p_i^+} \int \frac{d^3 k}{(2\pi)^3 2\omega} \int \frac{d^3 p}{(2\pi)^3 2E} \int \frac{d^4 q}{(2\pi)^4} g^4 t_c t_a t_c I \end{aligned} \quad (\text{C13})$$

where

$$\begin{aligned} I &= \int \prod_{i=0}^5 d^4 x_i \theta(x_1^+ - x_0^+) \theta(x_2^+ - x_1^+) \theta(x_3^+ - x_2^+) \theta(2L - (x_2^+ - x_0^+)) \theta(x_4^+ - x_5^+) \\ &\quad \times e^{-ip_3 \cdot (x_1 - x_0)} e^{-ik \cdot (x_4 - x_1)} e^{-ip_2 \cdot (x_2 - x_1)} e^{-i(p_1 + q) \cdot (x_3 - x_2)} e^{-ip \cdot (x_4 - x_3)} e^{-ip_4 \cdot (x_5 - x_4)} J(x_0) J(x_5) \\ &\quad \times (p_2 + p_3)^\mu P_{\mu\nu}(k) (p_+ p_4)^\nu (p_1 + p_2)^\rho D_{\rho\sigma}^>(q) (p + p_1)^\sigma \\ &= |J(p)|^2 (2\pi)^3 \delta((p_3 - p_2 - k)^+) \delta^2(\mathbf{p}_3 - \mathbf{p}_2 - \mathbf{k}) (2\pi)^3 \delta((p_2 - p)^+) \delta^2(\mathbf{p}_2 - \mathbf{p}) \\ &\quad \times (2\pi)^3 \delta((p_1 - p + q)^+) \delta^2(\mathbf{p}_1 - \mathbf{p} + \mathbf{q}) (2\pi)^3 \delta((p_4 - p - k)^+) \delta^2(\mathbf{p}_4 - \mathbf{p} - \mathbf{k}) I_1, \end{aligned} \quad (\text{C14})$$

and where

$$\begin{aligned} I_1 &= \int_0^{2L} dx_2'^+ e^{-\frac{i}{2}(p_2 - p)^- x_2'^+} \int_0^{x_2'^+} dx_1'^+ e^{-\frac{i}{2}(p_3 - p_2 - k)^- x_1'^+} \int_0^{\infty} dx_3'^+ e^{-\frac{i}{2}(p_1 - p + q)^- x_3'^+} \\ &\quad \times \int_0^{\infty} dx_4'^+ e^{\frac{i}{2}(p_4 - p - k)^- x_4'^+} (p_2 + p_3)^\mu P_{\mu\nu}(k) (p_+ p_4)^\nu (p_1 + p_2)^\rho D_{\rho\sigma}^>(q) (p + p_1)^\sigma. \end{aligned} \quad (\text{C15})$$

Here we defined $x_1' = x_1 - x_0$, $x_2' = x_2 - x_0$, $x_3' = x_3 - x_2$, $x_4' = x_4 - x_5$.

By using Eq. (B5) and by applying the δ functions from Eq. (C14), we obtain the following relations:

$$\begin{aligned} p_2^- &= p^- \rightarrow (p_2 - p)^- = 0, \\ p_3^- &= p_4^- = \frac{(\mathbf{p} + \mathbf{k})^2 + M^2}{(p + k)^+} \approx \frac{M^2}{E^+}, \\ (p + k - p_3)^- &= \xi(T), \\ (p_1 - p + q)^- &\approx q^-. \end{aligned} \quad (\text{C16})$$

Using Eqs. (B9) and (B10), Eq. (C15) can be written as

$$\begin{aligned}
I_1 &= 4 \int_0^L dl_2 \int_0^{2l_2} dx_1' e^{\frac{i}{2}\xi(T)x_1'} \int_0^\infty dl_3 e^{-i(p_1-p+q)^-l_3} \int_0^\infty dx_4' e^{-\frac{i}{2}\xi(T)x_4'} \left(\frac{-4\mathbf{k}^2}{x^2} \right) \theta \left(1 - \frac{q_0^2}{\mathbf{q}^2} \right) \\
&\quad \times \frac{T}{q_0} E^{+2} \frac{\mathbf{q}^2}{\mathbf{q}^2} 2 \operatorname{Im} \left(\frac{1}{q^2 - \Pi_L(q, T)} - \frac{1}{q^2 - \Pi_T(q, T)} \right) \\
&= \int_0^L dl_2 \left(1 - e^{i\xi(T)l_2} \right) \int_0^\infty dl_3 e^{-iq^-l_3} G(q, T(l_2)),
\end{aligned} \tag{C17}$$

where $G(q, T)$ is defined in Eq. (B15).

By using Eqs. (C13), (C14) and (C17), $M_{1,0,2,R}$ becomes

$$\begin{aligned}
M_{1,0,2,R} &= \int_0^L dl_2 \left(1 - e^{i\xi(T)l_2} \right) \int_0^\infty dl_3 e^{-iq^-l_3} \int \frac{d^3p}{(2\pi)^3 2E} |J(p)|^2 \int \frac{d^3k}{(2\pi)^3 2\omega} (-4) g^4 t_c t_a t_a t_c \\
&\quad \times \frac{\mathbf{k}^2}{(\mathbf{k}^2 + \chi(T))^2} \frac{1}{E^{+2}} \int \frac{d^4q}{(2\pi)^4} F(q_0, q_z, \mathbf{q}, T).
\end{aligned} \tag{C18}$$

Similarly, $M_{1,0,2,L}$ can be computed as

$$\begin{aligned}
M_{1,0,2,L} &= \int_0^L dl_2 \left(1 - e^{-i\xi(T)l_2} \right) \int_0^\infty dl_3 e^{iq^-l_3} \int \frac{d^3p}{(2\pi)^3 2E} |J(p)|^2 \int \frac{d^3k}{(2\pi)^3 2\omega} (-4) g^4 t_c t_a t_a t_c \\
&\quad \times \frac{\mathbf{k}^2}{(\mathbf{k}^2 + \chi(T))^2} \frac{1}{E^{+2}} \int \frac{d^4q}{(2\pi)^4} F(q_0, q_z, \mathbf{q}, T).
\end{aligned} \tag{C19}$$

Therefore, $M_{1,0,2,R} + M_{1,0,2,L}$ becomes

$$M_{1,0,2,R} + M_{1,0,2,L} = -4g^4 t_c t_a t_a t_c \int \frac{d^3p}{(2\pi)^3 2E} |J(p)|^2 \int \frac{d^3k}{(2\pi)^3 2\omega} \frac{1}{E^{+2}} I_2, \tag{C20}$$

where

$$\begin{aligned}
I_2 &= \left(\int_0^L dl_2 \left(1 - e^{i\xi(T)l_2} \right) \int_0^\infty dl_3 e^{-iq^-l_3} + \int_0^L dl_2 \left(1 - e^{-i\xi(T)l_2} \right) \int_0^\infty dl_3 e^{iq^-l_3} \right) \frac{\mathbf{k}^2}{(\mathbf{k}^2 + \chi(T))^2} \\
&\quad \times \int \frac{d^4q}{(2\pi)^4} F(q_0, q_z, \mathbf{q}, T) \\
&= \left(\frac{1}{2} \int_0^L dl_2 \left(2 - e^{i\xi(T)l_2} - e^{-i\xi(T)l_2} \right) \int_{-\infty}^\infty dl_3 e^{-iq^-l_3} + i \int_0^L dl_2 \left(e^{i\xi(T)l_2} - e^{-i\xi(T)l_2} \right) \right. \\
&\quad \left. \times \int_0^\infty dl_3 \sin(q^-l_3) \right) \frac{\mathbf{k}^2}{(\mathbf{k}^2 + \chi(T))^2} \int \frac{d^4q}{(2\pi)^4} F(q_0, q_z, \mathbf{q}, T) \\
&= \left(\frac{1}{2} \int_0^L dl_2 \left(2 - e^{i\xi(T)l_2} - e^{-i\xi(T)l_2} \right) 2\pi \delta(q^-) + i \int_0^L dl_2 \left(e^{i\xi(T)l_2} - e^{-i\xi(T)l_2} \right) \int_0^\infty dl_3 \sin(q^-l_3) \right) \\
&\quad \times \frac{\mathbf{k}^2}{(\mathbf{k}^2 + \chi(T))^2} \int \frac{d^4q}{(2\pi)^4} F(q_0, q_z, \mathbf{q}, T).
\end{aligned} \tag{C21}$$

Finally, by using Eqs. (C21), Eq. (C20) becomes

$$\begin{aligned}
& M_{1,0,2,R} + M_{1,0,2,L} = \\
& = - \int_0^L dl_2 \left(2 - e^{i\xi(T)l_2} - e^{-i\xi(T)l_2} \right) \int \frac{d^3p}{(2\pi)^3 2E} |J(p)|^2 \int \frac{d^3k}{(2\pi)^3 2\omega} 2g^4 t_c t_a t_a t_c \frac{\mathbf{k}^2}{(\mathbf{k}^2 + \chi(T))^2} I_q(T) \\
& -i \int_0^L dl_2 \left(e^{i\xi(T)l_2} - e^{-i\xi(T)l_2} \right) \int \frac{d^3p}{(2\pi)^3 2E} |J(p)|^2 \int \frac{d^3k}{(2\pi)^3 2\omega} 4g^4 t_c t_a t_a t_c \frac{\mathbf{k}^2}{(\mathbf{k}^2 + \chi(T))^2} K_q(T), \quad (C22)
\end{aligned}$$

where $I_q(T)$ is given in Eq. (B25), and $K_q(T)$ is given by

$$K_q(T) = \int_0^\infty dl_3 \int \frac{dq_0 dq_z d^2q}{(2\pi)^4} (\sin(q_0 l_3) \cos(q_z l_3) - \cos(q_0 l_3) \sin(q_z l_3)) F(q_0, q_z, \mathbf{q}, T), \quad (C23)$$

$F(q_0, q_z, \mathbf{q}, T)$ is even function of both q_0 and q_z , leading to

$$\begin{aligned}
& \int_{-\infty}^{\infty} dq_0 \sin(q_0 l_3) F(q_0, q_z, \mathbf{q}, T) = 0, \\
& \int_{-\infty}^{\infty} dq_z \sin(q_z l_3) F(q_0, q_z, \mathbf{q}, T) = 0. \quad (C24)
\end{aligned}$$

Therefore, we have

$$K_q(T) = 0. \quad (C25)$$

Finally, by using Eqs. (B25) and (C25), Eq. (C22) becomes

$$\begin{aligned}
M_{1,0,2,R} + M_{1,0,2,L} & = -4t_c t_a t_a t_c \int_0^L d\tau \int \frac{d^3p}{(2\pi)^3 2E} |J(p)|^2 \int \frac{d^3k}{(2\pi)^3 2\omega} \int \frac{d^2q}{(2\pi)^2} g^4 T v(q, T) \\
& \times \frac{\mathbf{k}^2}{(\mathbf{k}^2 + \chi(T))^2} \left(1 - \cos(\xi(T)\tau) \right). \quad (C26)
\end{aligned}$$

Appendix D: Calculation of Diagrams $M_{1,0,3,C}$ and $M_{1,0,4,C}$

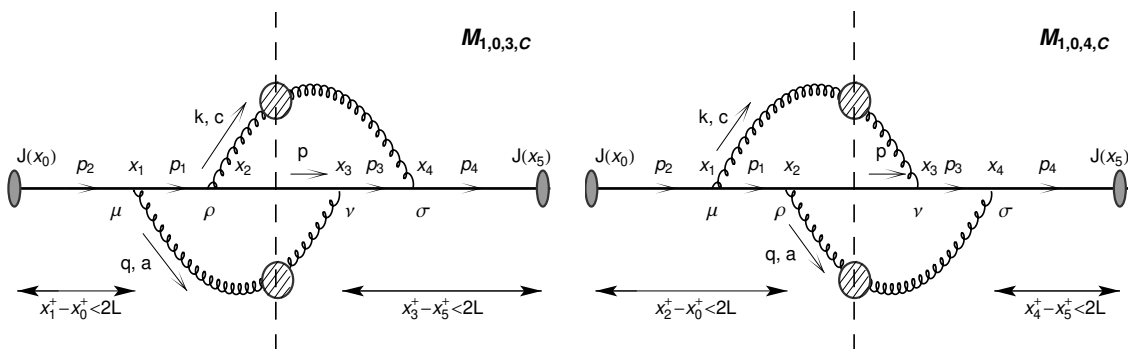


FIG. 3: Feynman diagrams $M_{1,0,3,C}$ and $M_{1,0,4,C}$, labeled in the same way as Fig. 1.

In this Appendix, we compute the cut diagrams $M_{1,0,3,C}$ and $M_{1,0,4,C}$, shown in Fig. 3. We start with $M_{1,0,3,C}$:

$$\begin{aligned}
M_{1,0,3,C} = & \int \prod_{i=0}^5 d^4 x_i J(x_0) \Delta_{++}^+(x_1 - x_0) v_\mu^+(x_1) D_{-+}^{\mu\nu}(x_3 - x_1) \Delta_{++}^+(x_2 - x_1) v_\rho^+(x_2) D_{-+}^{\rho\sigma}(x_4 - x_2) \\
& \times \Delta_{-+}(x_3 - x_2) v_\nu^-(x_3) \Delta_{--}^-(x_4 - x_3) v_\sigma^-(x_4) \Delta_{--}^-(x_5 - x_4) J(x_5) \\
& \times \theta(x_1^+ - x_0^+) \theta(x_2^+ - x_1^+) \theta(2L - (x_1 - x_0)^+) \theta(x_4^+ - x_3^+) \theta(x_3^+ - x_4^+) \theta(2L - (x_3 - x_5)^+).
\end{aligned} \tag{D1}$$

Following Appendix B and the first part of Appendix C, Eq. (D1) can be calculated as

$$\begin{aligned}
M_{1,0,3,C} = & -2t_a t_c t_a t_c \int_0^L d\tau \left(1 - e^{i\xi(T)\tau}\right) \int \frac{d^3 p}{(2\pi)^3 2E} |J(p)|^2 \int \frac{d^3 k}{(2\pi)^3 2\omega} \int \frac{d^2 q}{(2\pi)^2} g^4 T v(q, T) \\
& \times \frac{\mathbf{k}^2}{(\mathbf{k}^2 + \chi(T))^2}.
\end{aligned} \tag{D2}$$

Since $M_{1,0,4,C}$ is a complex conjugate of $M_{1,0,3,C}$, we obtain

$$\begin{aligned}
M_{1,0,3,C} + M_{1,0,4,C} = & -4t_a t_c t_a t_c \int_0^L d\tau \int \frac{d^3 p}{(2\pi)^3 2E} |J(p)|^2 \int \frac{d^3 k}{(2\pi)^3 2\omega} \int \frac{d^2 q}{(2\pi)^2} g^4 T v(q, T) \\
& \times \frac{\mathbf{k}^2}{(\mathbf{k}^2 + \chi(T))^2} \left(1 - \cos(\xi(T)\tau)\right).
\end{aligned} \tag{D3}$$

Appendix E: Calculation of Diagrams $M_{1,0,3,R}$ and $M_{1,0,4,L}$

The cut diagram $M_{1,0,3,R}$ shown in the left panel of Fig. 4 can be calculated as

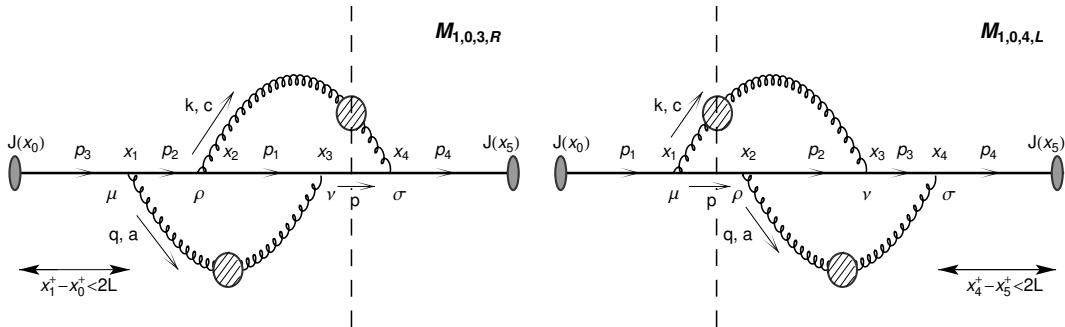


FIG. 4: Feynman diagrams $M_{1,0,3,R}$ and $M_{1,0,4,L}$, labeled in the same way as Fig. 1.

$$\begin{aligned}
M_{1,0,3,R} &= \int \prod_{i=0}^5 d^4 x_i J(x_0) \Delta_{++}^+(x_1 - x_0) v_\mu^+(x_1) D_{++}^{+\mu\nu}(x_3 - x_1) \Delta_{++}^+(x_2 - x_1) v_\rho^+(x_2) D_{-+}^{\rho\sigma}(x_4 - x_2) \\
&\times \Delta_{++}^+(x_3 - x_2) v_\lambda^+(x_3) \Delta_{-+}(x_4 - x_3) v_\sigma^-(x_4) \Delta_{--}^-(x_5 - x_4) J(x_5) \\
&\times \prod_{i=0}^3 \theta(x_{i+1}^+ - x_i^+) \theta(x_4^+ - x_5^+) \theta(2L - (x_1 - x_0)^+)
\end{aligned} \tag{E1}$$

Following Appendix F of Ref. [38], it can be shown that

$$M_{1,0,3,R} + M_{1,0,4,L} \approx 0. \tag{E2}$$

Appendix F: Calculation of Diagrams $M_{1,0,5,R}$ and $M_{1,0,6,L}$

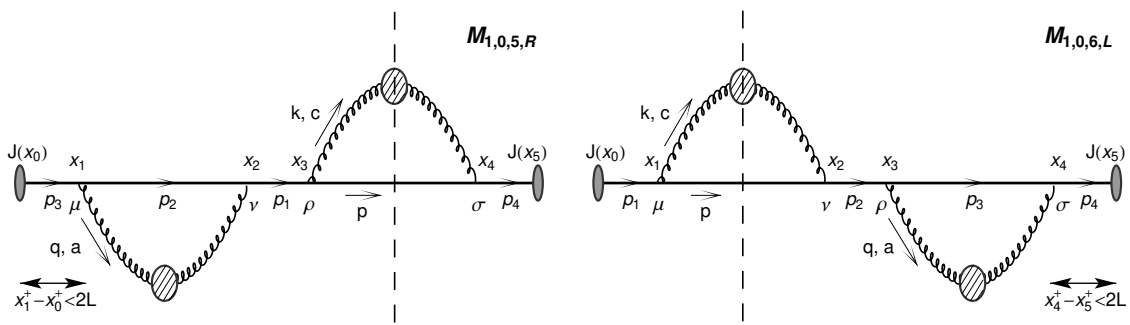


FIG. 5: Feynman diagrams $M_{1,0,5,R}$ and $M_{1,0,6,L}$, labeled in the same way as Fig. 1.

In this Appendix, we calculate the cut diagrams $M_{1,0,5,R}$ and $M_{1,0,6,L}$, shown in Fig. 5. We begin with $M_{1,0,5,R}$:

$$\begin{aligned}
M_{1,0,5,R} &= \int \prod_{i=0}^5 d^4 x_i J(x_0) \Delta_{++}^+(x_1 - x_0) v_\mu^+(x_1) D_{++}^{+\mu\nu}(x_2 - x_1) \Delta_{++}^+(x_2 - x_1) v_\nu^+(x_2) \\
&\times \Delta_{++}^+(x_3 - x_2) v_\rho^+(x_3) D_{-+}^{\rho\sigma}(x_4 - x_3) \Delta_{-+}(x_4 - x_3) v_\sigma^-(x_4) \Delta_{--}^-(x_5 - x_4) J(x_5) \\
&\times \theta(x_1^+ - x_0^+) \theta(x_2^+ - x_1^+) \theta(x_3^+ - x_2^+) \theta(x_5^+ - x_4^+) \theta(2L - (x_1 - x_0)^+).
\end{aligned} \tag{F1}$$

Following the computation of $M_{1,0,2,R}$ in Appendix C, Eq. (F1) becomes

$$\begin{aligned}
M_{1,0,5,R} &= -4t_a t_a t_c t_c \int_0^L dl_1 e^{i\xi(T)l_1} \int_0^\infty dl_2 e^{-iq^-l_2} \int \frac{d^3 p}{(2\pi)^3 2E} |J(p)|^2 \int \frac{d^3 k}{(2\pi)^3 2\omega} \\
&\times \frac{\mathbf{k}^2}{(\mathbf{k}^2 + \chi(T))^2} \int \frac{d^4 q}{(2\pi)^4} \theta\left(1 - \frac{q_0^2}{\mathbf{q}^2}\right) g^4 \frac{T}{q_0} \frac{\mathbf{q}^2}{\mathbf{q}^2} 2 \text{Im} \left(\frac{1}{q^2 - \Pi_L(q, T)} - \frac{1}{q^2 - \Pi_T(q, T)} \right)
\end{aligned} \tag{F2}$$

Since $M_{1,0,6,L}$ is the complex conjugate of $M_{1,0,5,R}$, we obtain

$$M_{1,0,5,R} + M_{1,0,6,L} = -4t_a t_a t_c t_c \int_0^L d\tau \int \frac{d^3 p}{(2\pi)^3 2E} |J(p)|^2 \int \frac{d^3 k}{(2\pi)^3 2\omega} \int \frac{d^2 q}{(2\pi)^2} g^4 T v(q, T) \times \frac{\mathbf{k}^2}{(\mathbf{k}^2 + \chi(T))^2} \cos(\xi(T)\tau). \quad (\text{F3})$$

Appendix G: Calculation of Diagrams $M_{1,1,1,C}$ and $M_{1,1,2,C}$

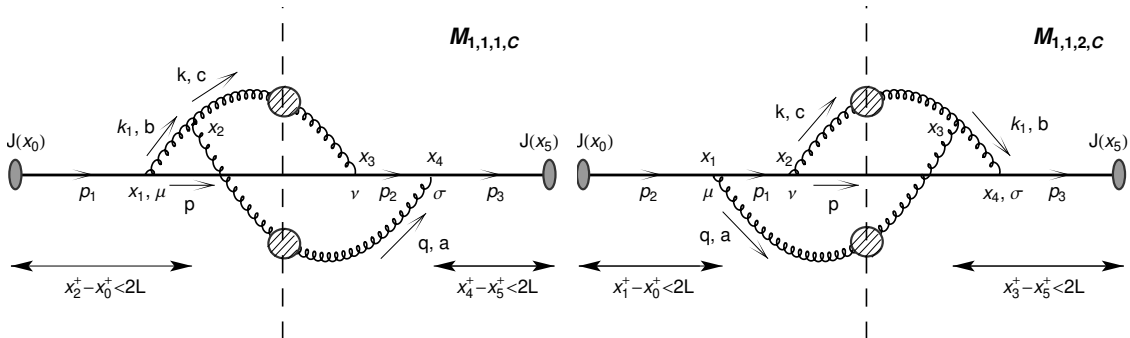


FIG. 6: Feynman diagrams $M_{1,1,1,C}$ and $M_{1,1,2,C}$, labeled in the same way as Fig. 1.

In Appendices G - J, we calculate the diagrams where one end of the exchanged gluon q is attached to the high- p_\perp parton, while the other end is connected to the radiated gluon k . Consequently, a 3-gluon vertex is involved in the diagrams. Here, we present the calculation of the diagrams shown in Fig. 6, starting with the cut diagram $M_{1,1,1,C}$:

$$\begin{aligned} M_{1,1,1,C} &= \int \prod_{i=0}^5 dx_i J(x_0) \Delta_{++}^+(x_1 - x_0) v_\mu^+(x_1) D_{++}^{+\mu\rho_1}(x_2 - x_1) v_{\rho_1\rho_2\rho_3}^+(x_2) \Delta_{-+}(x_3 - x_1) \\ &\quad \times D_{-+}^{\rho_3\nu}(x_3 - x_2) v_\nu^-(x_3) D_{-+}^{\rho_2\sigma}(x_4 - x_2) v_\sigma^-(x_4) \Delta_{--}^-(x_4 - x_3) \Delta_{--}^-(x_5 - x_4) J(x_5) \\ &\quad \times \theta(x_1^+ - x_0^+) \theta(x_2^+ - x_1^+) \theta(2L - (x_2 - x_0)^+) \theta(x_3^+ - x_4^+) \theta(x_4^+ - x_5^+) \\ &\quad \times \theta(2L - (x_4 - x_5)^+) \\ &= - \int_{-\infty}^{\infty} \int_0^{\infty} \prod_{i=1}^3 \frac{dp_i^+ d^2 p_i}{(2\pi)^3 2p_i^+} \frac{dk_1^+ d^2 k_1}{(2\pi)^3 2k_1^+} \int \frac{d^3 k}{(2\pi)^3 2\omega} \frac{d^3 p}{(2\pi)^3 2E} \frac{d^4 q}{(2\pi)^4} (-i) g^4 f^{cba} t_c t_b t_a I, \quad (\text{G1}) \end{aligned}$$

where

$$\begin{aligned}
I &= \int \prod_{i=0}^5 dx_i \theta(x_1^+ - x_0^+) \theta(x_2^+ - x_1^+) \theta(2L - (x_2 - x_0)^+) \theta(x_3^+ - x_4^+) \theta(x_4^+ - x_5^+) \\
&\quad \times \theta(2L - (x_4 - x_5)^+) e^{-ip_1(x_1-x_0)} e^{-ik_1(x_2-x_1)} e^{-ip(x_3-x_1)} e^{-ik(x_3-x_2)} e^{-iq(x_4-x_2)} \\
&\quad \times e^{-ip_2(x_4-x_3)} e^{-ip_3(x_5-x_4)} J(x_0) J(x_5) (p+p_1)^\mu P_{\mu\rho_1}(k_1) \left(g^{\rho_1\rho_3}(k_1+k)^{\rho_2} \right. \\
&\quad \left. + g^{\rho_2\rho_3}(q-k)^{\rho_1} + g^{\rho_1\rho_2}(-k_1-q)^{\rho_3} \right) P_{\rho_3\nu}(k) D_{\rho_2\sigma}^>(q) (p+p_2)^\nu (p_2+p_3)^\sigma \\
&= |J(p)|^2 (2\pi)^3 \delta((p_1-p-k_1)^+) \delta^2(\mathbf{p}_1-\mathbf{p}-\mathbf{k}_1) (2\pi)^3 \delta((k_1-k-q)^+) \delta^2(\mathbf{k}_1-\mathbf{k}-\mathbf{q}) \\
&\quad \times (2\pi)^3 \delta((p+k-p_2)^+) \delta^2(\mathbf{p}+\mathbf{k}-\mathbf{p}_2) (2\pi)^3 \delta((p+k+q-p_1)^+) \delta^2(\mathbf{p}+\mathbf{k}+\mathbf{q}-\mathbf{p}_1) I_1
\end{aligned} \tag{G2}$$

and where

$$\begin{aligned}
I_1 &= \int_0^{2L} dx_2'^+ e^{-\frac{i}{2}(k_1-k-q)^- x_2'^+} \int_0^{x_2'^+} dx_1'^+ e^{-\frac{i}{2}(p_1-p-k_1)^- x_1'^+} \int_0^\infty dx_3'^+ e^{-\frac{i}{2}(p+k-p_2)^- x_3'^+} \\
&\quad \times \int_0^{2L} dx_4'^+ e^{-\frac{i}{2}(p+k+q-p_3)^- x_4'^+} (p+p_1)^\mu P_{\mu\rho_1}(k_1) \left(g^{\rho_1\rho_3}(k_1+k)^{\rho_2} + g^{\rho_2\rho_3}(q-k)^{\rho_1} \right. \\
&\quad \left. + g^{\rho_1\rho_2}(-k_1-q)^{\rho_3} \right) P_{\rho_3\nu}(k) D_{\rho_2\sigma}^>(q) (p+p_2)^\nu (p_2+p_3)^\sigma \\
&= \frac{4}{(p_2-p-k)^-(p_1-p-k_1)^-} \int_0^{2L} dx_2'^+ e^{-\frac{i}{2}(k_1-k-q)^- x_2'^+} \left(1 - e^{-\frac{i}{2}(p_1-k_1-p)^- x_2'^+} \right) \\
&\quad \times \int_0^{2L} dx_4'^+ e^{-\frac{i}{2}(p+k+q-p_3)^- x_4'^+} (p+p_1)^\mu P_{\mu\rho_1}(k_1) \left(g^{\rho_1\rho_3}(k_1+k)^{\rho_2} + g^{\rho_2\rho_3}(q-k)^{\rho_1} \right. \\
&\quad \left. + g^{\rho_1\rho_2}(-k_1-q)^{\rho_3} \right) P_{\rho_3\nu}(k) D_{\rho_2\sigma}^>(q) (p+p_2)^\nu (p_2+p_3)^\sigma.
\end{aligned} \tag{G3}$$

Now we compute

$$\begin{aligned}
&(p_1+p_2)^\mu (p+p_2)^\nu (p_2+p_3)^\sigma P_{\mu\rho_1}(k_1) P_{\rho_3\nu}(k) D_{\rho_2\sigma}^>(q) \left(g^{\rho_1\rho_3}(k+k_1)^{\rho_2} + g^{\rho_2\rho_3}(q-k)^{\rho_1} \right. \\
&\quad \left. + g^{\rho_1\rho_2}(-k_1-q)^{\rho_3} \right) \\
&\approx \{ (p_1+p_2)^\mu P_{\mu\rho_1}(k_1) P_{\nu}^{\rho_1}(k) (p+p_2)^\nu \} \{ (k+k_1)^\rho D_{\rho\sigma}^>(q) (p_2+p_3)^\sigma \} \\
&\approx \left(-4 \frac{\mathbf{k} \cdot \mathbf{k}_1}{x^2} \right) \theta \left(1 - \frac{q_0^2}{\mathbf{q}^2} \right) \frac{T}{q_0} E^+ k^+ \frac{\mathbf{q}^2}{\mathbf{q}^2} 2 \operatorname{Im} \left(\frac{1}{q^2 - \Pi_L(q, T)} - \frac{1}{q^2 - \Pi_T(q, T)} \right).
\end{aligned} \tag{G4}$$

Therefore, I_1 can be written as

$$\begin{aligned}
I_1 &= \frac{16}{(p_2-p-k)^-(p_1-p-k_1)^-} \int_0^L dl_2 e^{-i(k_1-k-q)^- l_2} \left(1 - e^{-i(p_1-k_1-p)^- l_2} \right) \\
&\quad \times \int_0^L dl_4 e^{-i(p+k+q-p_3)^- l_4} \left(-4 \frac{\mathbf{k} \cdot \mathbf{k}_1}{x^2} \right) \theta \left(1 - \frac{q_0^2}{\mathbf{q}^2} \right) \frac{T}{q_0} E^+ k^+ \frac{\mathbf{q}^2}{\mathbf{q}^2} \\
&\quad \times 2 \operatorname{Im} \left(\frac{1}{q^2 - \Pi_L(q, T)} - \frac{1}{q^2 - \Pi_T(q, T)} \right) \\
&= \int_0^L dl_2 e^{-i(k_1-k-q)^- l_2} \left(1 - e^{-i(p_1-k_1-p)^- l_2} \right) \int_0^L dl_4 e^{-i(p+k+q-p_3)^- l_4} H(q, T(l_2)),
\end{aligned} \tag{G5}$$

where T is again associated with l_2 , and

$$H(q, T(l_2)) = \frac{16}{(p_2 - p - k)^-(p_1 - p - k_1)^-} \left(-4 \frac{\mathbf{k} \cdot \mathbf{k}_1}{x^2} \right) \theta \left(1 - \frac{q_0^2}{\mathbf{q}^2} \right) \frac{T}{q_0} E^+ k^+ \frac{\mathbf{q}^2}{\mathbf{q}^2} \\ \times 2 \operatorname{Im} \left(\frac{1}{q^2 - \Pi_L(q, T)} - \frac{1}{q^2 - \Pi_T(q, T)} \right). \quad (\text{G6})$$

By using Eq. (B5) and applying the δ functions from Eq. (G2), we obtain

$$p_1^- = p_3^- = \frac{M^2}{p_1^+} = \frac{M^2}{(p + k + q)^+}, \quad (\text{G7})$$

$$p^- = \frac{(\mathbf{k} + \mathbf{q})^2 + M^2}{p^+}, \quad k^- = \frac{\mathbf{k}^2 + m_g(T)^2}{k^+}, \quad k_1^- = \frac{(\mathbf{k} + \mathbf{q})^2 + m_g(T)^2}{(k + q)^+}, \quad p_2^- = \frac{\mathbf{q}^2 + M^2}{(p + k)^+}, \quad (\text{G8})$$

leading to

$$(p + k - p_2)^- = \frac{k^2 + \chi}{xE} \equiv \xi(T), \quad (\text{G9})$$

$$(p_1 - k_1 - p)^- \approx -\frac{(\mathbf{k} + \mathbf{q})^2 + \chi(T)}{xE} \equiv -\zeta(T), \quad (\text{G10})$$

$$(p + k + q - p_1)^- \approx q^-, \quad (\text{G11})$$

$$(k_1 - k - q)^- \approx -q^-. \quad (\text{G12})$$

Using these approximations, we obtain

$$I_1 = \int_0^L dl_2 e^{-i(k_1 - k - q)^- l_2} \left(1 - e^{-i(p_1 - k_1 - p)^- l_2} \right) 2\pi \delta(q_0 - q_z) H(q, T(l_2)). \quad (\text{G13})$$

Additionally, we note that

$$-i f^{abc} t_a t_b t_c = \frac{1}{2} [t_a, t_c] [t_c, t_a]. \quad (\text{G14})$$

Finally, by using Eqs. (B24), (G13), and (G14), Eq. (G1) reduces to

$$M_{1,1,1,C} = -2 [t_a, t_c] [t_c, t_a] \int_0^L dl_2 \left(1 - e^{i\zeta(T)l_2} \right) \int \frac{d^3 p}{(2\pi)^3 2E} |J(p)|^2 \int \frac{d^3 k}{(2\pi)^3 2\omega} \int \frac{d^2 q}{(2\pi)^2} \\ \times g^4 T v(q, T) \frac{\mathbf{k} \cdot (\mathbf{k} + \mathbf{q})}{(\mathbf{k}^2 + \chi(T)) ((\mathbf{k} + \mathbf{q})^2 + \chi(T))}. \quad (\text{G15})$$

As $M_{1,1,2,C}$ is the complex conjugate of $M_{1,1,1,C}$, one finally obtains

$$M_{1,1,1,C} + M_{1,1,2,C} = -4 [t_a, t_c] [t_c, t_a] \int_0^L d\tau \int \frac{d^3 p}{(2\pi)^3 2E} |J(p)|^2 \int \frac{d^3 k}{(2\pi)^3 2\omega} \int \frac{d^2 q}{(2\pi)^2} g^4 T v(q, T) \\ \times \frac{\mathbf{k} \cdot (\mathbf{k} + \mathbf{q})}{(\mathbf{k}^2 + \chi(T)) ((\mathbf{k} + \mathbf{q})^2 + \chi(T))} \left(1 - \cos(\zeta(T)\tau) \right). \quad (\text{G16})$$

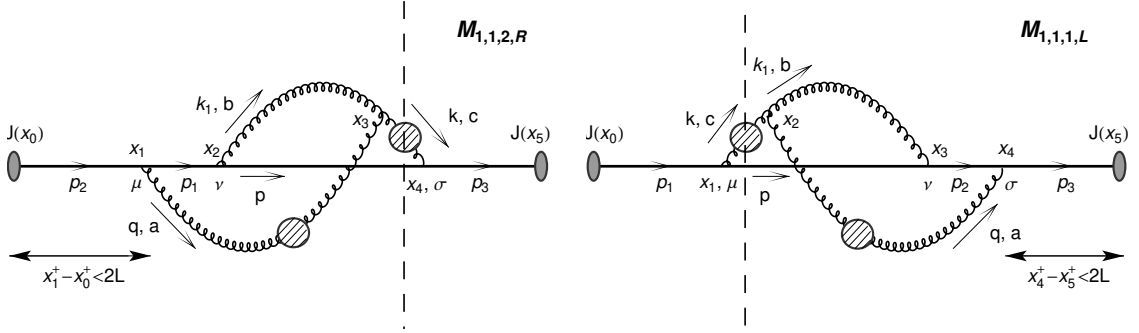


FIG. 7: Feynman diagrams $M_{1,1,2,R}$ and $M_{1,1,1,L}$, labeled in the same way as Fig. 1.

Appendix H: Calculation of Diagrams $M_{1,1,2,R}$ and $M_{1,1,1,L}$

The cut diagram $M_{1,1,2,R}$, shown in the left panel of Fig. 7, can be calculated as

$$\begin{aligned}
 M_{1,1,2,R} = & \int \prod_{i=0}^5 dx_i J(x_0) \Delta_{++}^+(x_1 - x_0) v_{\mu}^+(x_1) D_{++}^{+\mu\rho_2}(x_3 - x_1) v_{\rho_1\rho_2\rho_3}^+(x_3) \Delta_{++}^+(x_2 - x_1) \\
 & \times D_{++}^{\rho_1\nu}(x_3 - x_2) v_{\nu}^+(x_2) D_{-+}^{\rho_3\sigma}(x_4 - x_2) v_{\sigma}^-(x_4) \Delta_{-+}(x_4 - x_2) v_{--}^-(x_5 - x_4) J(x_5) \\
 & \times \theta(x_1^+ - x_0^+) \theta(x_2^+ - x_1^+) \theta(2L - (x_1 - x_0)^+) \theta(x_3^+ - x_2^+) \theta(x_4^+ - x_5^+). \quad (\text{H1})
 \end{aligned}$$

By applying the same procedure as in Appendix I in Ref. [38], we obtain

$$M_{1,1,1,L} + M_{1,1,2,R} = 0. \quad (\text{H2})$$

Appendix I: Calculation of Diagrams $M_{1,1,3,C}$ and $M_{1,1,4,C}$

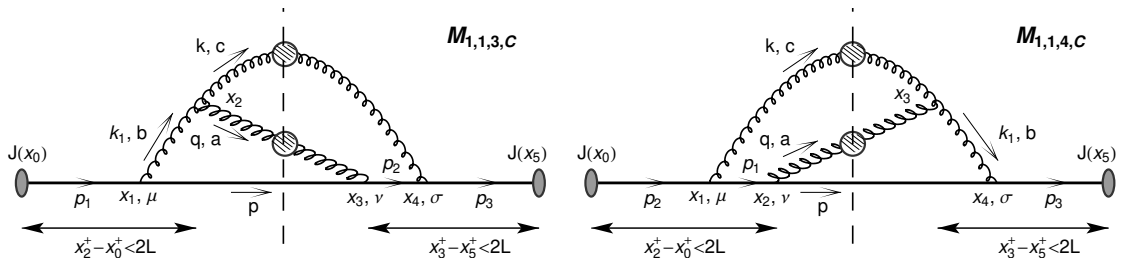


FIG. 8: Feynman diagrams $M_{1,1,3,C}$ and $M_{1,1,4,C}$, labeled in the same way as Fig. 1.

We here calculate the cut diagrams $M_{1,1,3,C}$ and $M_{1,1,4,C}$, shown in Fig. 8. $M_{1,1,3,C}$ can be computed as

$$\begin{aligned}
M_{1,1,3,C} &= \int \prod_{i=0}^5 dx_i J(x_0) \Delta_{++}^+(x_1 - x_0) v_\mu^+(x_1) D_{++}^{+\mu\rho_1}(x_2 - x_1) v_{\rho_1\rho_2\rho_3}^+(x_2) \Delta_{-+}(x_3 - x_1) \\
&\times D_{-+}^{\rho_2\lambda}(x_3 - x_2) v_\lambda^-(x_3) \Delta_{--}^-(x_4 - x_3) D_{-+}^{\rho_3\sigma}(x_4 - x_2) v_\sigma^-(x_4) \Delta_{--}^-(x_5 - x_4) J(x_5) \\
&\times \int_{-\infty}^{\infty} \int_0^{\infty} \frac{dp_3^+ d^2 p_3}{(2\pi)^3 2p_3^+} e^{-ip_3(x_5 - x_4)} (ig(p_2 + p_3)^\sigma t_b) J(x_5) \theta(x_1^+ - x_0^+) \theta(x_2^+ - x_1^+) \\
&\times \theta(2L - (x_2 - x_0)^+) \theta(x_3^+ - x_4^+) \theta(x_4^+ - x_5^+) \theta(2L - (x_3 - x_5)^+). \tag{I1}
\end{aligned}$$

Similar to Appendix G, Eq. (I1) can be calculated as

$$\begin{aligned}
M_{1,1,3,C} &= -2[t_a, t_c][t_c, t_a] \int_0^L d\tau \left(1 - e^{i\zeta(T)\tau} - e^{-i\xi(T)\tau} - e^{i(\zeta(T) - \xi(T))\tau}\right) \int \frac{d^3 p}{(2\pi)^3 2E} |J(p)|^2 \\
&\times \int \frac{d^3 k}{(2\pi)^3 2\omega} \int \frac{d^2 q}{(2\pi)^2} g^4 T v(q, T) \frac{\mathbf{k} \cdot (\mathbf{k} + \mathbf{q})}{(\mathbf{k}^2 + \chi(T))((\mathbf{k} + \mathbf{q})^2 + \chi(T))}. \tag{I2}
\end{aligned}$$

Since $M_{1,1,4,C}$ is the complex conjugate of $M_{1,1,3,C}$, one obtains

$$\begin{aligned}
&M_{1,1,3,C} + M_{1,1,4,C} \\
&= -4[t_a, t_c][t_c, t_a] \int_0^L d\tau \int \frac{d^3 p}{(2\pi)^3 2E} |J(p)|^2 \int \frac{d^3 k}{(2\pi)^3 2\omega} \int \frac{d^2 q}{(2\pi)^2} g^4 T v(q, T) \\
&\times \frac{\mathbf{k} \cdot (\mathbf{k} + \mathbf{q})}{(\mathbf{k}^2 + \chi(T))((\mathbf{k} + \mathbf{q})^2 + \chi(T))} [1 - \cos(\zeta(T)\tau) - \cos(\xi(T)\tau) + \cos((\zeta(T) - \xi(T))\tau)]. \tag{I3}
\end{aligned}$$

Appendix J: Calculation of Diagrams $M_{1,1,3,R}$, $M_{1,1,3,L}$, $M_{1,1,4,L}$, and $M_{1,1,4,R}$

In this Appendix, we calculate the cut diagrams $M_{1,1,3,R}$, $M_{1,1,3,L}$, $M_{1,1,4,R}$, and $M_{1,1,4,L}$ shown in Fig. 9. $M_{1,1,3,R}$ can be calculated as

$$\begin{aligned}
M_{1,1,3,R} &= \int \prod_{i=0}^5 dx_i J(x_0) \Delta_{++}^+(x_1 - x_0) v_\mu^+(x_1) D_{++}^{+\mu\rho_1}(x_2 - x_1) v_{\rho_1\rho_2\rho_3}^+(x_2) \Delta_{++}^+(x_3 - x_1) \\
&\times D_{++}^{+\rho_2\nu}(x_3 - x_2) v_\nu^+(x_3) D_{-+}^{\rho_3\sigma}(x_4 - x_2) v_\sigma^-(x_4) \Delta_{-+}(x_4 - x_3) \Delta_{--}^-(x_5 - x_4) J(x_5) \\
&\times \theta(x_1^+ - x_0^+) \theta(x_2^+ - x_1^+) \theta(2L - (x_2 - x_0)^+) \theta(x_3^+ - x_2^+) \theta(x_4^+ - x_5^+) \\
&\approx - \int_{-\infty}^{\infty} \int_0^{\infty} \prod_{i=1}^3 \frac{dp_i^+ d^2 p_i}{(2\pi)^3 2p_i^+} \frac{dk_1^+ d^2 k_1}{(2\pi)^3 2k_1^+} \int \frac{d^3 k}{(2\pi)^3 2\omega} \frac{d^3 p}{(2\pi)^3 2E} \frac{d^4 q}{(2\pi)^4} (-i) g^4 f^{cba} t_c t_b t_a I, \tag{J1}
\end{aligned}$$

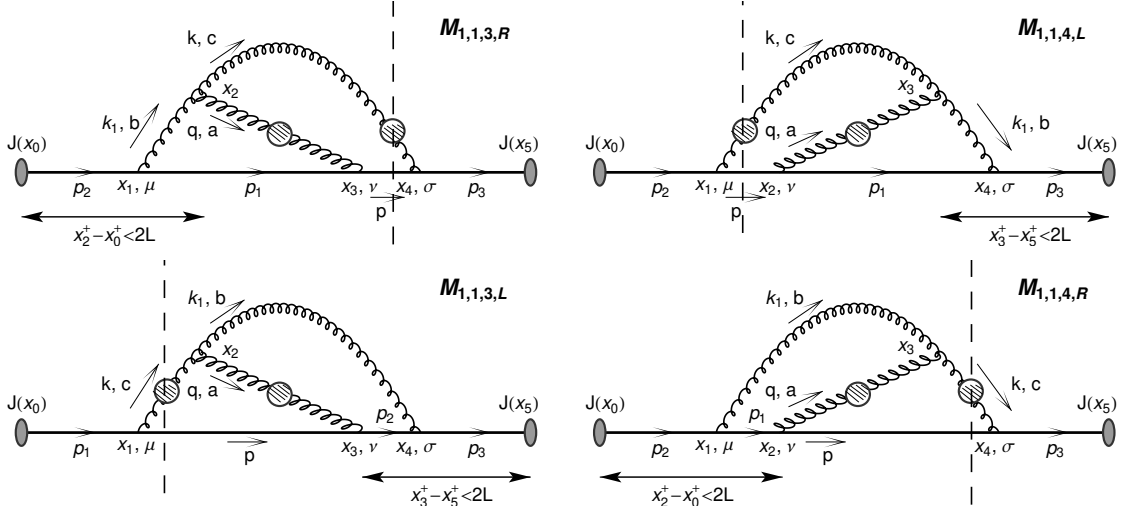


FIG. 9: Feynman diagrams $M_{1,1,3,R}$, $M_{1,1,3,L}$, $M_{1,1,4,R}$ and $M_{1,1,4,L}$, labeled in the same way as Fig. 1.

where

$$\begin{aligned}
I &= \int \prod_{i=0}^5 dx_i \theta(x_1^+ - x_0^+) \theta(x_2^+ - x_1^+) \theta(2L - (x_2 - x_0)^+) \theta(x_3^+ - x_2^+) \theta(x_4^+ - x_5^+) \\
&\times e^{-ip_2(x_1-x_0)} e^{-ik_1(x_2-x_1)} e^{-ip_1(x_3-x_1)} e^{-iq(x_3-x_2)} e^{-ik(x_4-x_2)} e^{-ip(x_4-x_3)} e^{-ip_3(x_5-x_4)} \\
&\times J(x_0) J(x_5) (p_1 + p_2)^\mu (p + p_1)^\nu (p + p_3)^\sigma P_{\mu\rho_1}(k_1) D_{\rho_2\nu}^>(q) P_{\rho_3\sigma}(k) \left(g^{\rho_1\rho_3} (k_1 + k)^{\rho_2} \right. \\
&+ \left. g^{\rho_2\rho_3} (q - k)^{\rho_1} + g^{\rho_1\rho_2} (-k_1 - q)^{\rho_3} \right) \\
&= |J(p)|^2 (2\pi)^3 \delta((p_2 - p_1 - k_1)^+) \delta^2(\mathbf{p}_2 - \mathbf{p}_1 - \mathbf{k}_1) (2\pi)^3 \delta((k_1 - k + p_1 - p)^+) \\
&\times \delta^2(\mathbf{k}_1 - \mathbf{k} + \mathbf{p}_1 - \mathbf{p}) (2\pi)^3 \delta((p_1 + q - p)^+) \delta^2(\mathbf{p}_1 + \mathbf{q} - \mathbf{p}) (2\pi)^3 \delta((p_3 - p - k)^+) \\
&\times \delta^2(\mathbf{p}_3 - \mathbf{p} - \mathbf{k}) I_1,
\end{aligned} \tag{J2}$$

where

$$\begin{aligned}
I_1 &= \int_0^{2L} dx_2'^+ e^{-\frac{i}{2}(k_1 - k + p_1 - p)^- x_2'^+} \int_0^{x_2'^+} dx_1'^+ e^{-\frac{i}{2}(p_2 - p_1 - k_1)^- x_1'^+} \int_0^\infty dx_3'^+ e^{-\frac{i}{2}(p_1 + q - p)^- x_3'^+} \\
&\times \int_0^\infty dx_4'^+ e^{\frac{i}{2}(p_3 - p - k)^- x_4'^+} (p_1 + p_2)^\mu (p + p_1)^\nu (p + p_3)^\sigma P_{\mu\rho_1}(k_1) D_{\rho_2\nu}^>(q) P_{\rho_3\sigma}(k) \\
&\times \left(g^{\rho_1\rho_3} (k_1 + k)^{\rho_2} + g^{\rho_2\rho_3} (q - k)^{\rho_1} + g^{\rho_1\rho_2} (-k_1 - q)^{\rho_3} \right).
\end{aligned} \tag{J3}$$

Using the following relation

$$\begin{aligned}
& (p_1 + p_2)^\mu (p + p_1)^\nu (p + p_3)^\sigma P_{\mu\rho_1}(k_1) D_{\rho_2\nu}^>(q) P_{\rho_3\sigma}(k) \left(g^{\rho_1\rho_3} (k_1 + k)^{\rho_2} + g^{\rho_2\rho_3} (q - k)^{\rho_1} \right. \\
& \left. + g^{\rho_1\rho_2} (-k_1 - q)^{\rho_3} \right) \\
& \approx \{ (p_1 + p_2)^\mu P_{\mu\rho_1}(k_1) P_{\sigma}^{\rho_1}(k) (p + p_3)^\sigma \} \{ (k + k_1)^{\rho_2} D_{\rho_2\nu}^>(q) (p + p_1)^\nu \} \\
& \approx -\frac{4\mathbf{k} \cdot (\mathbf{k} + \mathbf{q})}{x^2} \theta \left(1 - \frac{q_0^2}{\mathbf{q}^2} \right) \frac{T}{q_0} E^+ k^+ \frac{\mathbf{q}^2}{\mathbf{q}^2} 2 \text{Im} \left(\frac{1}{q^2 - \Pi_L(q, T)} - \frac{1}{q^2 - \Pi_T(q, T)} \right)
\end{aligned} \tag{J4}$$

in Eq. (J3), one obtains

$$\begin{aligned}
I_1 &= \int_0^{2L} dx_2'^+ e^{-\frac{i}{2}(k_1 - k + p_1 - p)^- x_2'^+} \int_0^{x_2'^+} dx_1'^+ e^{-\frac{i}{2}(p_2 - p_1 - k_1)^- x_1'^+} \int_0^\infty dx_3'^+ e^{-\frac{i}{2}(p_1 + q - p)^- x_3'^+} \\
&\times \int_0^\infty dx_4'^+ e^{\frac{i}{2}(p_3 - p - k)^- x_4'^+} \left(-\frac{4\mathbf{k} \cdot (\mathbf{k} + \mathbf{q})}{x^2} \right) \theta \left(1 - \frac{q_0^2}{\mathbf{q}^2} \right) \frac{T}{q_0} E^+ k^+ \frac{\mathbf{q}^2}{\mathbf{q}^2} \\
&\times 2 \text{Im} \left(\frac{1}{q^2 - \Pi_L(q, T)} - \frac{1}{q^2 - \Pi_T(q, T)} \right).
\end{aligned} \tag{J5}$$

By using Eq. (B6) and the δ functions from Eq. (J2), we obtain, under the soft gluon and soft rescattering approximation,

$$\begin{aligned}
p_2^- &= p_3^- = \frac{M^2}{E^+}, \\
(p_2 - p_1 - k_1)^- &= -\zeta(T), \\
(p_3 - p - k)^- &= (p_2 - p - k)^- = -\xi(T), \\
(k_1 - k + p_1 - p)^- &= \zeta(T) - \xi(T), \\
(q + p_1 - p)^- &\approx q_0 - q_z.
\end{aligned} \tag{J6}$$

Using Eq. (J6), Eq. (J5) becomes

$$I_1 = \int_0^L dl_2 \left(e^{-i(\zeta(T) - \xi(T))l_2} - e^{i\xi(T)l_2} \right) \int_0^\infty dl_3 e^{-iq^- l_3} H(q, T(l_2)), \tag{J7}$$

where $H(q, T(l_2))$ is defined in Eq. (G6).

Finally, by using Eqs. (G6) and (J7), Eq. (J1) reduces to

$$\begin{aligned}
M_{1,1,3,R} &= 2 [t_a, t_c] [t_c, t_a] \int_0^L dl_2 \left(e^{-i(\zeta(T) - \xi(T))l_2} - e^{i\xi(T)l_2} \right) \int_0^\infty dl_3 e^{-iq^- l_3} \int \frac{d^3 p}{(2\pi)^3 2E} |J(p)|^2 \\
&\times \int \frac{d^3 k}{(2\pi)^3 2\omega} \int \frac{d^4 q}{(2\pi)^4} \frac{\mathbf{k} \cdot (\mathbf{k} + \mathbf{q})}{((\mathbf{k} + \mathbf{q})^2 + \chi(T)) ((\mathbf{k}^2 + \chi(T))} \theta \left(1 - \frac{q_0^2}{\mathbf{q}^2} \right) g^4 \frac{T}{q_0} \frac{\mathbf{q}^2}{\mathbf{q}^2} \\
&\times 2 \text{Im} \left(\frac{1}{q^2 - \Pi_L(q, T)} - \frac{1}{q^2 - \Pi_T(q, T)} \right).
\end{aligned} \tag{J8}$$

$M_{1,1,4,L}$ is the complex conjugate of $M_{1,1,3,R}$. Moreover, the relationship $M_{1,1,3,L} + M_{1,1,4,R} = M_{1,1,3,R} + M_{1,1,4,L}$ holds, leading to the final result.

$$\begin{aligned}
& M_{1,1,3,L} + M_{1,1,3,R} + M_{1,1,4,R} + M_{1,1,4,L} = \\
& = 4 [t_a, t_c] [t_c, t_a] \int_0^L d\tau \int \frac{d^3 p}{(2\pi)^3 2E} |J(p)|^2 \int \frac{d^3 k}{(2\pi)^3 2\omega} \int \frac{d^2 q}{(2\pi)^2} g^4 T v(q, T) \\
& \quad \times \frac{\mathbf{k} \cdot (\mathbf{k} + \mathbf{q})}{((\mathbf{k} + \mathbf{q})^2 + \chi(T)) (\mathbf{k}^2 + \chi(T))} \left(\cos((\xi(T) - \zeta(T))\tau) - \cos(\xi(T)\tau) \right). \quad (\text{J9})
\end{aligned}$$

Appendix K: Calculation of Diagram $M_{1,2,C}$

In Appendices K and L, we calculate the diagrams where both ends of the exchanged gluon q are attached to the radiated gluon k , involving two 3-gluon vertices in the process. Here, we compute the diagram $M_{1,2,C}$ shown in Fig. 10.

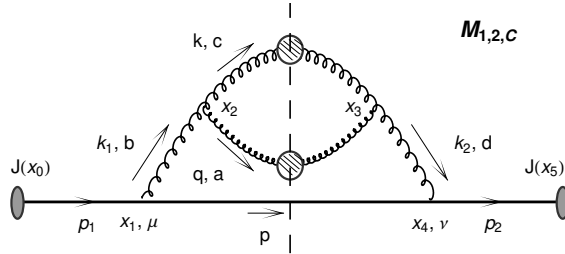


FIG. 10: Feynman diagram $M_{1,2,C}$, labeled in the same way as Fig. 1.

$$\begin{aligned}
M_{1,2,C} &= \int \prod_{i=0}^5 dx_i J(x_i) \Delta_{++}^+(x_1 - x_0) v_{\mu}^+(x_1) D_{++}^{+\mu\rho_1}(x_2 - x_1) v_{\rho_1\rho_2\rho_3}^+(x_2) D_{-+}^{\rho_3\sigma_3}(x_3 - x_2) \\
&\quad \times D_{-+}^{\rho_2\sigma_2}(x_3 - x_2) \Delta_{-+}(x_4 - x_3) v_{\sigma_1\sigma_2\sigma_3}^-(x_3) D_{--}^{-\sigma_1\nu}(x_4 - x_3) v_{\nu}^-(x_4) \Delta_{--}^-(x_5 - x_4) J(x_5) \\
&\quad \times \theta(x_1^+ - x_0^+) \theta(x_2^+ - x_1^+) \theta(2L - (x_2 - x_0)^+) \theta(x_3^+ - x_4^+) \theta(x_4^+ - x_5^+) \\
&\quad \times \theta(2L - (x_3 - x_5)^+). \quad (\text{K1})
\end{aligned}$$

Following Appendix G and applying the following relations:

$$\begin{aligned}
& (p + p_1)^{\mu} P_{\mu\rho_1}(k_1) P^{\sigma_1\rho_1}(k) P_{\sigma\nu}(k_2) (p + p_1)^{\nu} = (p + p_1)^{\mu} P_{\mu\rho_1}(k_1) P^{\sigma_1\rho_1}(k) P_{\sigma_1\nu}(k_1) (p + p_1)^{\nu} \\
& \quad \approx -\frac{4(\mathbf{k} + \mathbf{q})^2}{x^2} \\
& (k + k_1)^{\rho_2} D_{\rho_2\sigma_2}^>(q, T) (k + k_2)^{\sigma_2} \approx k^+ k_1^+ \theta \left(1 - \frac{q_0^2}{\mathbf{q}^2} \right) \frac{T}{q_0} \frac{\mathbf{q}^2}{\mathbf{q}^2} 2 \text{Im} \left(\frac{1}{q^2 - \Pi_L(q, T)} - \frac{1}{q^2 - \Pi_T(q, T)} \right) \quad (\text{K2})
\end{aligned}$$

Eq. (K1) becomes

$$M_{1,2,C} = 8 [t_a, t_c] [t_c, t_a] \int_0^L d\tau \int \frac{d^3 p}{(2\pi)^3 2E} |J(p)|^2 \int \frac{d^3 k}{(2\pi)^3 2\omega} \int \frac{d^2 q}{(2\pi)^2} g^4 T v(q, T) \times \frac{(\mathbf{k} + \mathbf{q})^2}{((\mathbf{k} + \mathbf{q})^2 + \chi(T))^2} (1 - \cos(\zeta(T)\tau)). \quad (\text{K3})$$

Appendix L: Calculation of Diagrams $M_{1,2,R}$ and $M_{1,2,L}$

In this Appendix, we calculate the cut diagrams $M_{1,2,R}$ and $M_{1,2,L}$ shown in Fig. 11. We start with $M_{1,2,R}$:

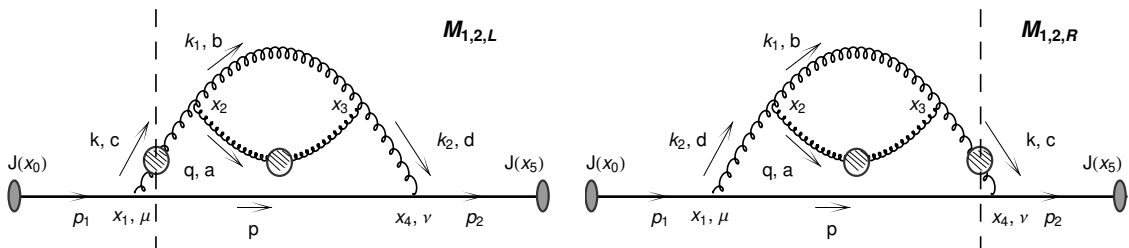


FIG. 11: Feynman diagrams $M_{1,2,L}$ and $M_{1,2,R}$ labeled in the same way as Fig. 1.

$$M_{1,2,R} = \int \prod_{i=0}^5 dx_i J(x_0) \Delta_{++}^+(x_1 - x_0) v_{\mu}^+(x_1) D_{++}^{+\mu\rho_1}(x_2 - x_1) v_{\rho_1\rho_2\rho_3}^+(x_2) D_{++}^{+\rho_3\sigma_3}(x_3 - x_2) \times D_{++}^{+\rho_2\sigma_2}(x_3 - x_2) \Delta_{-+}(x_4 - x_1) v_{\sigma_1\sigma_2\sigma_3}^+(x_3) D_{-+}^{\sigma_1\nu}(x_4 - x_3) v_{\nu}^-(x_4) \Delta_{--}^-(x_5 - x_4) J(x_5) \times \theta(x_1^+ - x_0^+) \theta(x_2^+ - x_1^+) \theta(x_3^+ - x_2^+) \theta(x_4^+ - x_3^+) \theta(2L - (x_2 - x_0)). \quad (\text{L1})$$

Equation (L1) can be computed by following Appendix J and applying the following approximations:

$$(p + p_1)^\mu P_{\mu\rho_1}(k_2) P^{\rho_1\sigma_1}(k) P_{\sigma_1\nu}(k) (p + p_2)^\nu = -\frac{4\mathbf{k}^2}{\xi(T)^2} (k + k_1)^\rho D_{\rho\sigma}^>(q, T) (k + k_1)^\sigma \approx k^+ k_1^+ \theta\left(1 - \frac{q_0^2}{\mathbf{q}^2}\right) \frac{T}{q_0} \frac{\mathbf{q}^2}{\mathbf{q}^2} 2 \text{Im} \left(\frac{1}{q^2 - \Pi_L(q, T)} - \frac{1}{q^2 - \Pi_T(q, T)} \right), \quad (\text{L2})$$

as

$$M_{1,2,R} = -4g^4 [t_c, t_a] [t_a, t_c] \int_0^L dl_2 \left(1 - e^{i\xi(T)l_2}\right) \int_0^\infty dl_3 e^{-iq^-l_3} \int \frac{d^3 p}{(2\pi)^3 2E} |J(p)|^2 \int \frac{d^3 k}{(2\pi)^3 2\omega} \times \int \frac{d^4 q}{(2\pi)^4} \frac{\mathbf{k}^2}{(\mathbf{k}^2 + \chi(T))^2} \theta\left(1 - \frac{q_0^2}{\mathbf{q}^2}\right) \frac{T}{q_0} \frac{\mathbf{q}^2}{\mathbf{q}^2} 2 \text{Im} \left(\frac{1}{q^2 - \Pi_L(q, T)} - \frac{1}{q^2 - \Pi_T(q, T)} \right). \quad (\text{L3})$$

As $M_{1,2,L}$ is a complex conjugate of $M_{1,2,R}$, one finally obtains

$$\begin{aligned}
 M_{1,2,R} + M_{1,2,L} = & -4 [t_a, t_c] [t_c, t_a] \int_0^L d\tau \int \frac{d^3 p}{(2\pi)^3 2E} |J(p)|^2 \int \frac{d^3 k}{(2\pi)^3 2\omega} \int \frac{d^2 q}{(2\pi)^2} g^4 T v(q, T) \\
 & \times \frac{\mathbf{k}^2}{(\mathbf{k}^2 + \chi(T))^2} (1 - \cos(\xi(T)\tau)). \tag{L4}
 \end{aligned}$$

-
- [1] E. V. Shuryak, Nucl. Phys. A **750**, 64 (2005); Rev. Mod. Phys. **89**, 035001 (2017).
 - [2] M. Gyulassy and L. McLerran, Nucl. Phys. A **750**, 30 (2005).
 - [3] B. Jacak and P. Steinberg, Phys. Today **63**, 39 (2010).
 - [4] B. Muller, J. Schukraft and B. Wyslouch, Ann. Rev. Nucl. Part. Sci. **62**, 361 (2012).
 - [5] R. Stock, Nature **337**, 319 (1989).
 - [6] S. Acharya *et al.* [ALICE], JHEP **11**, 013 (2018).
 - [7] S. Acharya *et al.* [ALICE], JHEP **01**, 174 (2022).
 - [8] [ATLAS], ATLAS-CONF-2017-012.
 - [9] V. Khachatryan *et al.* [CMS], JHEP **04**, 039 (2017).
 - [10] S. Acharya *et al.* [ALICE], JHEP **07**, 103 (2018).
 - [11] S. Acharya *et al.* [ALICE], Phys. Lett. B **813**, 136054 (2021).
 - [12] M. Aaboud, *et al.* [ATLAS], Eur. Phys. J. C **78**, 997 (2018).
 - [13] A. M. Sirunyan, *et al.* [CMS], Phys. Lett. B **776**, 195 (2018).
 - [14] A. M. Sirunyan *et al.* [CMS], Phys. Lett. B **816**, 136253 (2021).
 - [15] P. Achenbach, D. Adhikari, A. Afanasev, F. Afzal, C. A. Aidala, A. Al-bataineh, D. K. Almaalol, M. Amarian, D. Androić and W. R. Armstrong, *et al.* Nucl. Phys. A **1047**, 122874 (2024).
 - [16] L. Apolinário, Y. J. Lee and M. Winn, Prog. Part. Nucl. Phys. **127**, 103990 (2022).
 - [17] D. Zigic, J. Auvinen, I. Salom, M. Djordjevic and P. Huovinen, Phys. Rev. C **106**, 044909 (2022).
 - [18] D. Zigic, I. Salom, J. Auvinen, P. Huovinen and M. Djordjevic, Front. in Phys. **10**, 957019 (2022).
 - [19] D. Everett *et al.* [JETSCAPE], Phys. Rev. C **103**, 054904 (2021).
 - [20] D. Everett *et al.* [JETSCAPE], Phys. Rev. Lett. **126**, 242301 (2021).
 - [21] W. Fan *et al.* [JETSCAPE], Phys. Rev. C **107**, no.5, 054901 (2023).
 - [22] O. Soloveva, J. Aichelin and E. Bratkovskaya, Phys. Rev. D **105**, 054011 (2022).
 - [23] T. Song, H. Berrehrah, D. Cabrera, J. M. Torres-Rincon, L. Tolos, W. Cassing and E. Bratkovskaya, Phys. Rev. C **92**, no.1, 014910 (2015).
 - [24] W. J. Xing, S. Cao and G. Y. Qin, Phys. Lett. B **850**, 138523 (2024).
 - [25] Y. He, W. Chen, T. Luo, S. Cao, L. G. Pang and X. N. Wang, Phys. Rev. C **106**, no.4, 044904 (2022).
 - [26] S. Stojku, J. Auvinen, M. Djordjevic, P. Huovinen and M. Djordjevic, Phys. Rev. C **105**, L021901 (2022).
 - [27] S. Stojku, J. Auvinen, L. Zivkovic, P. Huovinen and M. Djordjevic, Phys. Lett. B **835**, 137501 (2022).

- [28] B. Karmakar, D. Zigic, M. Djordjevic, P. Huovinen, M. Djordjevic and J. Auvinen, Phys. Rev. C **110**, no.4, 044906 (2024).
- [29] B. Karmakar, D. Zigic, I. Salom, J. Auvinen, P. Huovinen, M. Djordjevic and M. Djordjevic, Phys. Rev. C **108**, no.4, 044907 (2023).
- [30] W. Ke and I. Vitev, Phys. Rev. C **107**, no.6, 064903 (2023).
- [31] Y. T. Chien, A. Emerman, Z. B. Kang, G. Ovanessian and I. Vitev, Phys. Rev. D **93**, no.7, 074030 (2016).
- [32] R. Baier, Y. Dokshitzer, A. Mueller, S. Peigne, and D. Schiff, Nucl.Phys.B **484**, 265 (1997).
- [33] B. Zakharov, JETP Lett. **63**, 952 (1996); *ibid* **65**, 615 (1997).
- [34] N. Armesto, C. A. Salgado, and U. A. Wiedemann, Phys. Rev. D **69**, 114003 (2004).
- [35] M. Gyulassy, P. Levai, and I. Vitev, Nucl. Phys. B **594**, 371 (2001).
- [36] M. Djordjevic and M. Gyulassy, Nucl. Phys. A **733**, 265 (2004).
- [37] P. Arnold, G. D. Moore and L. G. Yaffe, JHEP **11**, 057 (2001); JHEP **12**, 009 (2001).
- [38] M. Djordjevic, Phys. Rev. C **80**, 064909 (2009).
- [39] M. Djordjevic and U. Heinz, Phys. Rev. Lett. **101**, 022302 (2008).
- [40] W. Xin-Nian and X. Guo, Nucl. Phys. A **696** (2001).
- [41] A. Majumder and M. Van Leeuwen, Prog. Part. Nucl. Phys. **66** (2011).
- [42] C. Andres, L. Apolinário and F. Dominguez, JHEP **07**, 114 (2020).
- [43] C. Andres, F. Dominguez and M. Gonzalez Martinez, JHEP **03**, 102 (2021).
- [44] Y. Mehtar-Tani, JHEP **07**, 057 (2019).
- [45] Y. Mehtar-Tani and K. Tywoniuk, JHEP **06**, 187 (2020).
- [46] M. D. Sievert and I. Vitev, Phys. Rev. D **98**, 094010 (2018).
- [47] M. D. Sievert, I. Vitev and B. Yoon, Phys. Lett. B **795**, 502 (2019).
- [48] J. Barata, X. Mayo López, A. V. Sadofyev and C. A. Salgado, Phys. Rev. D **108**, no.3, 034018 (2023).
- [49] A. V. Sadofyev, M. D. Sievert and I. Vitev, SciPost Phys. Proc. **8**, 046 (2022)
- [50] B. Blagojevic and M. Djordjevic, J. Phys. G **42**, 075105 (2015).
- [51] A. Bazavov *et al.* [HotQCD Collaboration], Phys. Rev. D **90**, 094503 (2014)
- [52] M. Djordjevic and U. Heinz, Phys. Rev. C **77**, 024905 (2008).
- [53] J. I. Kapusta, *Finite-Temperature Field Theory* (Cambridge University Press, 1989).
- [54] M. Le Bellac, *Thermal Field Theory* (Cambridge University Press, 1996).
- [55] A. B. Migdal, Phys. Rev. **103**, 1811 (1956); L. D. Landau and I. Pomeranchuk, Dokl. Akad. Nauk Ser. Fiz. **92**, 535 and 735 (1953).
- [56] O. K. Kalashnikov and V. V. Klimov, Sov. J. Nucl. Phys. **31**, 699 (1980).
- [57] V. V. Klimov, Sov. Phys. JETP **55**, 199 (1982).
- [58] A. V. Selikhov, M. Gyulassy, Phys. Lett. B **316**, 373 (1993); and Phys. Rev. C **49**, 1726 (1994).
- [59] A. Rebhan, Lect. Notes Phys. **583**, 161 (2002);
- [60] M. Djordjevic, Phys. Rev. C **74**, 064907 (2006).
- [61] E. Braaten and M. H. Thoma, Phys. Rev. D **44**, R2625 (1991).

- [62] E. Braaten and M. H. Thoma, Phys. Rev. D **44**, 1298 (1991).
- [63] M. H. Thoma and M. Gyulassy, Nucl. Phys. B **351**, 491 (1991).
- [64] M. Djordjevic and M. Gyulassy, Phys. Rev. C **68**, 034914 (2003).
- [65] X. N. Wang, Phys. Lett. B **485**, 157 (2000).
- [66] Y. Maezawa *et al.* [WHOT-QCD], Phys. Rev. D **81** (2010), 091501.
- [67] A. Hart, M. Laine and O. Philipsen, Nucl. Phys. B **586** (2000), 443-474.
- [68] S. Borsányi, Z. Fodor, S. D. Katz, A. Pásztor, K. K. Szabó and C. Török, JHEP **04**, 138 (2015).
- [69] M. Djordjevic and M. Djordjevic, Phys. Lett. B **709** (2012), 229-233.
- [70] A. Peshier, [arXiv:hep-ph/0601119 [hep-ph]].
- [71] R. Field, Applications of Perturbative QCD, Perseus Books, Cambridge, Massachusetts (1995).
- [72] M. Djordjevic and M. Djordjevic, Phys. Lett. B **734**, 286-289 (2014).
- [73] J. B. Kogut, D. E. Soper, Phys. Rev. D **1**, 2901 (1970).